Neuron

Olfactory landmarks and path integration converge to form a cognitive spatial map

Highlights

- Localized odor cues can serve as landmarks to guide virtual navigation in the dark

- Evolution of the CA1 spatial map reflects iterative recognition of odor landmarks

- Path integration imposes spatial meaning on odor cues to establish them as landmarks

- A model reveals how odors and path integration interact to extend spatial maps

Authors

Walter Fischler-Ruiz, David G. Clark, Narendra R. Joshi, ..., Mark Schnitzer, L.F. Abbott, Richard Axel

Correspondence

lfa2103@columbia.edu (L.F.A.), ra27@columbia.edu (R.A.)

In brief

The recognition of a spatial landmark by its sensory features poses a problem for neural circuits. Fischler-Ruiz, et al. show how this problem is solved when mice use odor cues to navigate in the dark. In the hippocampus, path integration imposes spatial meaning on odor cues, thereby creating new landmarks.

CellPress

Article

Olfactory landmarks and path integration converge to form a cognitive spatial map

Walter Fischler-Ruiz,[1] David G. Clark,[1] Narendra R. Joshi,[1] Virginia Devi-Chou,[1] Lacey Kitch,[2,3] Mark Schnitzer,[2,3,4] L.F. Abbott,[1,5,*] and Richard Axel[1,6,7,8,*]

[1]Mortimer B. Zuckerman Mind Brain and Behavior Institute, Department of Neuroscience, Columbia University, New York, NY, 10027 USA
[2]James H. Clark Center for Biomedical Engineering & Sciences, Stanford University, Stanford, CA, 94305 USA
[3]CNC Program, Stanford University, Stanford, CA, 94305 USA
[4]Howard Hughes Medical Institute, Stanford University, Stanford, CA, 94305 USA
[5]Department of Physiology and Cellular Biophysics, Columbia University, New York, NY, 10032 USA
[6]Department of Biochemistry and Molecular Biophysics, Columbia University, New York, NY, 10032 USA
[7]Howard Hughes Medical Institute, Columbia University, New York, NY, 10027 USA
[8]Lead contact
*Correspondence: lfa2103@columbia.edu (L.F.A.), ra27@columbia.edu (R.A.)
https://doi.org/10.1016/j.neuron.2021.09.055

SUMMARY

The convergence of internal path integration and external sensory landmarks generates a cognitive spatial map in the hippocampus. We studied how localized odor cues are recognized as landmarks by recording the activity of neurons in CA1 during a virtual navigation task. We found that odor cues enriched place cell representations, dramatically improving navigation. Presentation of the same odor at different locations generated distinct place cell representations. An odor cue at a proximal location enhanced the local place cell density and also led to the formation of place cells beyond the cue. This resulted in the recognition of a second, more distal odor cue as a distinct landmark, suggesting an iterative mechanism for extending spatial representations into unknown territory. Our results establish that odors can serve as landmarks, motivating a model in which path integration and odor landmarks interact sequentially and iteratively to generate cognitive spatial maps over long distances.

INTRODUCTION

Path integration is a navigational strategy that allows animals to form an internal estimate of position relative to external landmarks (Etienne and Jeffery, 2004; Etienne et al., 1998; Etienne et al., 2004; Kim and Dickinson, 2017; Mittelstaedt and Mittelstaedt, 1980; 2001; Müller and Wehner, 1988). Path integration relies on idiothetic (self-motion) signals derived from vestibular, proprioceptive, visual flow, and motor sources, that provide imperfect estimates of movement. Accumulated errors in the internal estimate of position must be corrected by external landmarks (Etienne et al., 2004; Hardcastle et al., 2015). The convergence of path integration and external landmarks expands the range over which animals can accurately navigate.

The recognition of a landmark poses an interesting conceptual problem. The sensory features of a landmark have no inherent spatial meaning and are only valuable if they are recognized as fixed in space (Jeffery, 1998; Savelli and Knierim, 2019), and this determination may require path integration (Bourboulou et al., 2019; Campbell et al., 2018; Chen et al., 2013; Fattahi et al., 2018; Jayakumar et al., 2019; Müller and Wehner, 2010; Ravassard et al., 2013). A further problem of disambiguation emerges if the same sensory features are encountered at different locations (Draht et al., 2017; Grieves et al., 2016; Zhao

et al., 2020). The convergence of path integration and sensory features creates a cognitive spatial map that can impose unique spatial meanings on these features to create landmarks.

Odors are a primary source of sensory information and may serve as navigational landmarks if fixed in space (Aboitiz and Montiel, 2015; Baker et al., 2018; Hamburger and Knauff, 2019; Jacobs, 2012; Jacobs et al., 2015; Koutsoklenis and Papadopoulos, 2011; Marin et al., 2021; Nosal et al., 2016; Porter et al., 2007; Raithel and Gottfried, 2021; Steck et al., 2009; Wu et al., 2020). The hippocampus receives olfactory information from the lateral entorhinal cortex (LEC) (Leitner et al., 2016; Li et al., 2017; Woods et al., 2020). The LEC receives direct input from the olfactory bulb and piriform cortex, two structures that encode odor identity (Diodato et al., 2016; Sosulski et al., 2011; Stettler and Axel, 2009). The influence of odors on hippocampal activity has been observed in both spatial and nonspatial contexts (Aikath et al., 2014; Anderson and Jeffery, 2003; Igarashi et al., 2014; Li et al., 2017; MacDonald et al., 2013; Muzzio et al., 2009; Radvansky and Dombeck, 2018; Radvansky et al., 2021; Taxidis et al., 2020; Young et al., 1997). Grid (Hafting et al., 2005), head direction (Sargolini et al., 2006), and speed cells (Kropff et al., 2015) in the medial entorhinal cortex (MEC) are driven by internal path integration signals and provide information to the hippocampus about location and self-motion. In

the dark, these internal path integration signals, in combination with olfactory and/or tactile cues, are able to support stable spatial representations in the hippocampus (Kulvicius et al., 2008; Quirk et al., 1990; Save et al., 1998; Save et al., 2000; Zhang and Manahan-Vaughan, 2015; Zhang et al., 2014). Thus, the hippocampus is a potential site of convergence for internal path integration and external sensory landmarks.

We have examined the activity of hippocampal neurons in mice performing a navigation behavior that relies solely on path integration and sparse olfactory sensory cues. The results of these experiments demonstrate the convergence of path integration and landmarks in the formation of a cognitive spatial map in the hippocampus. These observations led to the formulation of a theoretical model to describe how path integration and olfactory landmarks interact in an iterative process to form a cognitive spatial map.

RESULTS

Accurate navigation behavior in the presence of olfactory landmarks

We designed a series of experiments that required mice to navigate in the dark toward a virtual goal location on the basis of path integration in combination with olfactory landmarks. Initially, mice were trained to traverse a distance of 4 m on a featureless spherical treadmill, while head-fixed, in total darkness to reach an unmarked goal location where they received a water reward (Figures 1A and S1A). The ball had a single rotational axis, rendering the task equivalent to navigation on a linear track. Initially, this task required mice to estimate their own location and that of the goal using only path integration based on internal idiothetic signals. In the absence of odors, behavioral performance plateaued after 1–2 weeks (n = 5 mice). Mice initiated licking and decreased their running speed after traveling only ~2 m along the 4-m track (Figures 1B, 1C, 1D, S1B, and S1C). Thus, in this paradigm, path integration alone may not permit accurate measurement of distances greater than ~2 m.

We then introduced two brief pulses of the same odor delivered when the mice reached locations at 1 m and 3 m (Figure 1E). Photoionization detector (PID) measurements revealed only ~1% differences in the time-varying odor concentrations resulting from the 1-m and 3-m pulses (Figure 1F). Trials using one of two neutral odor cues, limonene or pinene, were randomly interleaved. This task required the mice to determine their location solely on the basis of path integration and odor cues, allowing us to study the convergence of idiothetic self-motion and external olfactory information in the generation of cognitive spatial maps. After four days of training with odor cues, all mice suppressed licking and maintained high running speeds for ~3.5 m of travel, commencing licking and rapidly slowing their running speed ~0.5 m from the reward location (Figures 1C, 1D, 1G, S1B, S1C, SID, and S1E). This suggests that the mice recognized the odors as spatial landmarks and used these landmarks to improve navigation.

Olfactory landmarks enhance place cell representations in CA1

We used a miniature microscope (Ghosh et al., 2011; Ziv et al., 2013) (nVista 2.0, Inscopix) and the genetically encoded fluorescent Ca^{2+} indicator GCamp6f to image the somatic Ca^{2+} activity

of ~3,000 CA1 pyramidal neurons per session, pooled across mice. We identified individual neurons and their Ca^{2+} traces from the fluorescence videos and registered their activity to the trajectories of the mice on the virtual track. Neural and behavioral data were averaged in 100-mm bins for analysis. Neurons with consistent position-selective activity were classified as place cells (STAR Methods).

After 1–2 weeks of training without odor cues, 5.8% of the imaged neurons were classified as place cells (169 of 2893 neurons; Figures 2A–2C, S1G–S1I, and S2; Table S1A). The spatial density of place cells was maximal at the starting location and decayed rapidly with distance (length constant ± bootstrapped standard error: 0.97 ± 0.20 m; Figure 2D). Place field reliability decreased with distance from the start location, and place field jitter and width increased as the mice traversed the track (Figures 2E, S1H, and S1I). At the population level, the across-trial stability of the vector of population activity decreased with distance (0.44 ± 0.02 versus 0.23 ± 0.01; Figure 2F). These results show that, in this paradigm, path integration alone cannot support reliable place cell activity beyond ~2 m. The sparse and unreliable neural representation of space beyond ~2 m is consistent with the behavioral observation that the mice began to lick at ~2 m, perhaps reflecting error accumulation in path integration.

We next examined whether spatially localized odor cues enhance place cell representations. After mice performed the task with odor cues at 1 m and 3 m for 4 days, the percentage of place cells increased from 5.8% to 35% (979 of 2,778 neurons, union of limonene and pinene place cells; Figures 2G–2I, S1F, S1G, S1J, and S2; Table S1). The density of place cells showed an overall increase over the length of the track but was most pronounced slightly beyond 1 m and 3 m, the locations of odor exposure (Figure 2D). Importantly, different sets of place cells were active at 1 m and 3 m, despite exposure to the same odor at both locations. We also observe a relatively small population of neurons that respond at both sites of odor presentation (Figure 2J; 2.4%, 68 of 2,778 neurons) which were excluded from place cell analysis. The presence of three spaced peaks (at the start and two odor locations) allowed the place cell density to remain high along the entire track despite the decay between peaks. Place field reliability increased following odor training whereas place field jitter tended to decrease (Figures 2E and S1H). At the population level, the across-trial stability of the vector of population activity increased following odor training (0.36 ± 0.01 versus 0.61 ± 0.01; Figure 2F). The elevated place cell density and increase in reliability was consistent with the animals' ability to suppress licking and retain running speed up to the reward site when odor cues are present. The peak in place cells at the 3-m odor cue and elevated place cell density all the way up to the reward location are consistent with the use of a cognitive spatial map to support navigation.

Analysis of place cell activity on individual trials revealed a significant correlation between the number of place cells active at the 1-m and 3-m odor landmarks (Figures 2K and S1M)). This suggests that during spatial navigation, the density of place cells at a proximal landmark influences the density of place cells at a more distal location.

Upon decoding of position from CA1 population activity, we observe that mice largely adjusted their distance estimates and licking behavior in response to trial-by-trial velocity
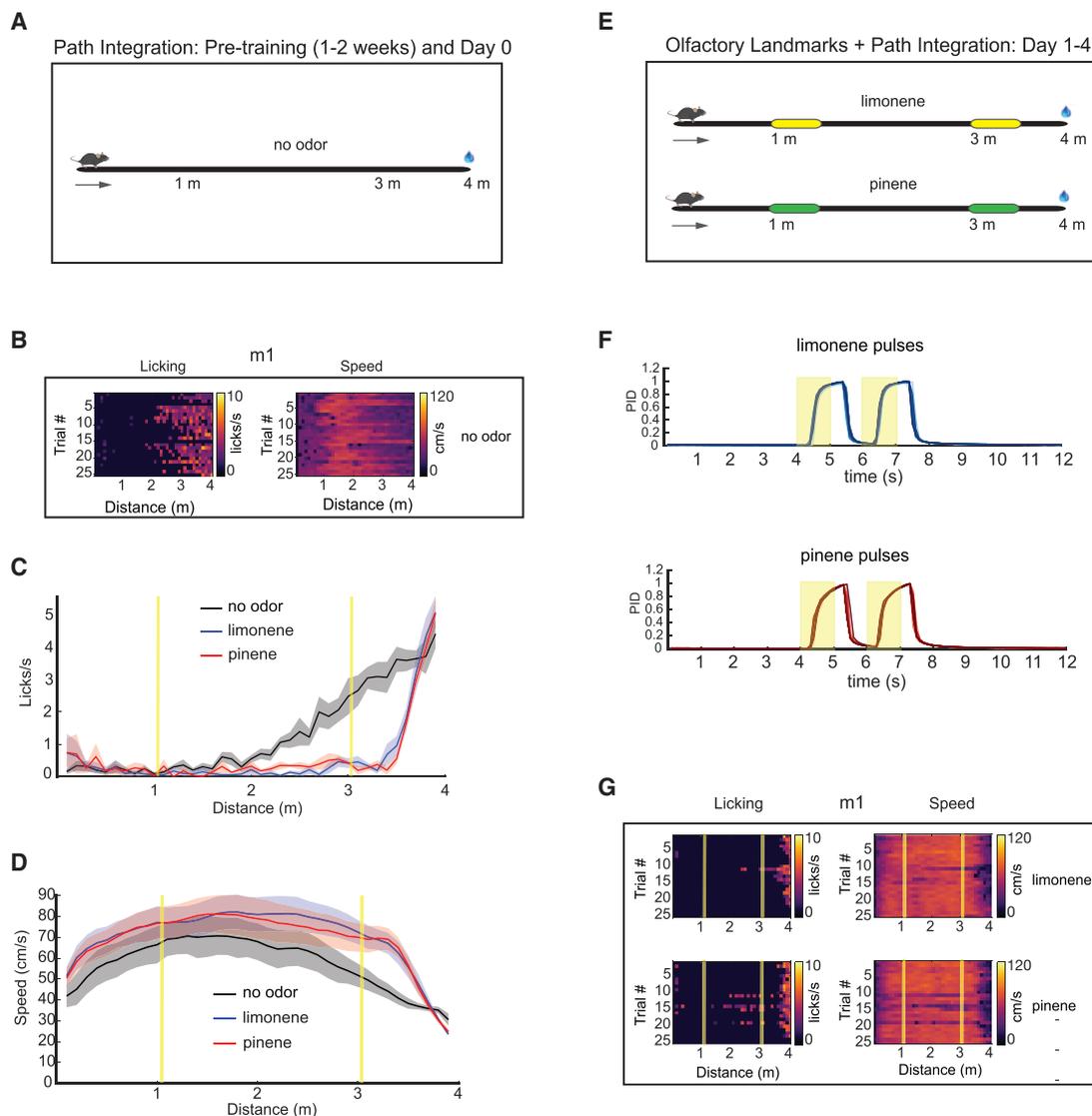
Figure 1. Accurate navigation behavior in the presence of olfactory landmarks

(A) Schematic of virtual track during training with no odor landmarks. During pre-training, the mice learned to run down a 4-m virtual linear track to receive a water reward. The number of pre-training sessions varied between 4 and 11 across mice. Behavioral data were recorded during the final 2 days of pre-training (days −2 and −1) in all mice. All data from n = 5 mice

(B) Single-trial behavioral data on day 0 (no odor cues) for an individual mouse (m1). Left, single-trial lick rate. Right, single-trial speed.

(C) Trial-average lick rate. Black, day 0, no odor cues. Blue, day 4, limonene trials. Red, day 4, pinene trials. Error bars: mean ± standard error across mice.

(D) Trial-average speed. Black, day 0, no odor cues. Blue, day 4, limonene trials. Red, day 4, pinene trials. Error bars: mean ± standard error across mice.

(E) Schematic of virtual track during training with odor landmarks.

(F) Plots of odor concentrations delivered in time by custom olfactometer. 1 s odor pulses were delivered with the minimum delay (1 s) between offset of 1st cue and onset of 2nd cue that was possible when mice ran at the fastest recorded speed (∼100cm/s). Shaded yellow areas indicate times at which odor valve is open. Top, 10% Limonene, blue traces. Bottom, 10% Pinene, red traces.
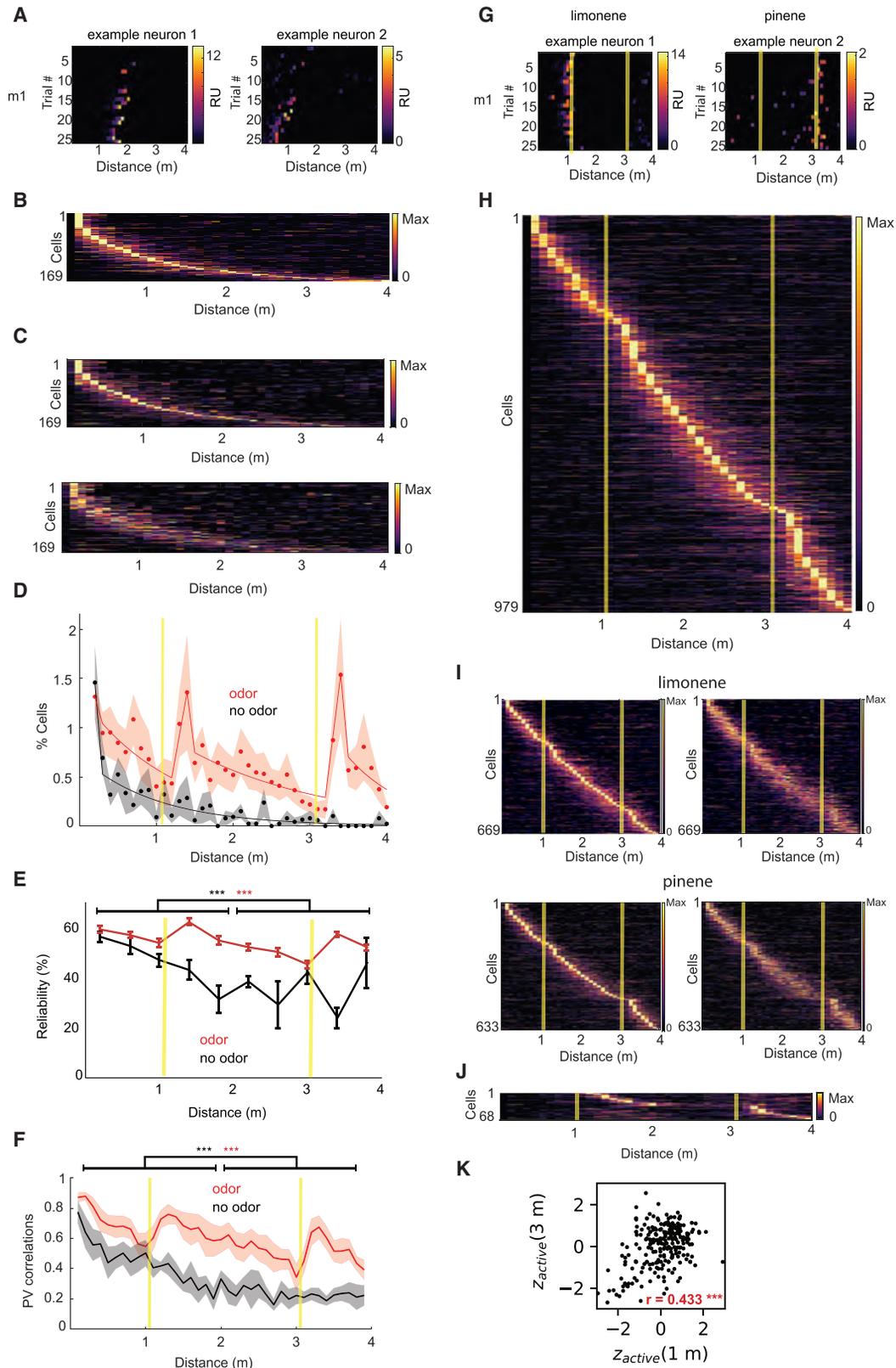
(G) Single-trial behavioral data on day 4 in the presence of odor landmarks for an individual mouse (m1). Left, single-trial lick rate. Right, single-trial speed.

deviations (Figures S3B–S3G; STAR Methods), showing a link between neural activity in CA1 and navigational behavior. Importantly, this shows that the animals perform the task using path integration to recognize the odor cues as spatial landmarks rather than employing estimates of elapsed time. Taken together, these results demonstrate that odor cues can serve as landmarks that couple with path integration to generate

robust spatially dependent neural activity that supports accurate navigational behavior.

Olfactory landmarks induce place cell remapping and generate distinct cognitive spatial maps

We examined whether different odors elicit different spatial maps by interleaving limonene and pinene trials. The two odors

A

example neuron 1   example neuron 2

m1

G

limonene   pinene

example neuron 1   example neuron 2

m1

B

Cells

C

Cells

Cells

H

Cells

D

% Cells

odor
no odor

I

limonene

Cells   Cells

pinene

Cells   Cells

E

Reliability (%)

*** ***

odor
no odor

J

Cells

F

*** ***

odor
no odor

K

z_{active}(3 m)

z_{active}(1 m)

r = 0.433 ***

(legend on next page)

generated different place cell representations, demonstrating remapping (Figure 3A). Beyond the first odor cue (1 m), only 11% of place cells (78 of 708 place cells) served as place cells at the same location in both limonene and pinene trials. In accord with these findings, the correlation between the trial-average vectors of population activity dropped from ~80% for the same odor to ~15% for different odors following the first odor cue and remained small beyond 1 m (Figure 3B). The re-mapping between limonene and pinene trials was observed as early as the first day of training in the presence of odor cues (Figure 3C). These data indicate that different odors at the same location in identical tasks generate distinct cognitive spatial maps.

The gradual and sequential emergence of place cell maps and improvement in navigation behavior

We further analyzed the interaction of path integration and odor cues by examining the emergence of place cells during training and the associated improvement in navigational behavior. On the first day of training in the presence of odor cues, mice initiated licking and decreased their running speed at ~2 m while briefly suppressing licking and increasing their running speed at the onset of the 3-m odor cue (Figures 4A and 4B). Over the three days of training, we observed a gradual reduction in licking and increase in running speed at locations that preceded the 3-m odor cue (Figures 4A and 4B). By the fourth day of training, mice avoided licking and maintained a high running speed up to the 3-m odor cue followed by a rapid increase in licking and decrease in speed after the odor cue and ~0.5 m from the reward location (Figures 4A and 4B). We quantified the anticipatory licking behavior by calculating a lick ratio, defined as the average lick rate within 0.3 m of reward divided by the average lick rate over the final 3 m of the virtual track (Methods). The lick ratio, averaged across mice, increased with each day of odor training following day 1 and we observed an increase in the lick ratio from 2.74 ± 0.18 to 7.14 ± 0.20 following all four days of odor training (Figures 4D and S3A). These observations suggest that the mice employ path integration to optimize their navigational behavior.

The evolution of the place cell representation mirrored the gradual improvement in navigational behavior. On the first day of training in the presence of odor cues, the spatial density of place cells increased locally at the 1-m odor cue, but not at the 3-m cue (Figures 4C, 4E, and S4A). Over subsequent days of training, the number and density of place cells progressively increased (Figures 4F, 4G, S4B, and S4C). Correspondingly, the error in the decoded estimate of position decreased more than 2-fold (0.46 m on day 1 to 0.22 m on day 4; Figure 4H; STAR Methods). Importantly, the emergence of a peak in the density of place cells at 1 m was accompanied by an increase in the density of place cells between 1 m and 3 m. Over the course of several days, as more place cells tiled the region between 1 m and 3 m, an additional peak in place cell density arose at 3 m. The emergence of peaks in place cell density at 1 m and 3 m was therefore gradual and sequential.

These results suggest an iterative process for spatial map extension in which increasingly distal sensory cues are recognized as landmarks. First, the odor cue nearest the start is recognized as a landmark, resulting in a local peak in place cell density. This leads to a gradual increase in place cell density beyond the first cue, allowing the mice to recognize a second odor cue as a distinct landmark. This, in turn, leads to an increase in place cell density beyond the second cue. This iterative process could be a

---

Figure 2. Olfactory landmarks enhance place cell representations in CA1

(A) Single-trial activity of two example neurons on day 0 (no odor cues) from mouse m1.

(B) Trial-average activity of place cells across all mice, sorted by place field centers, on day 0 (no odor cues).

(C) Cross-validation of place field ordering. Place cells were sorted by place field centers on odd trials. Top, odd-trial-average activity. Bottom, even-trial-average activity. day 0, no odor cues.

(D) Spatial density of place cells (number of place cells with centers in each spatial bin, divided by the total number of neurons). Black dots, day 0, no odor cues. Black line, exponential fit to the mouse-average density over 0.2–4 m. Red dots, day 4, combined limonene and pinene trials (limonene and pinene place cell densities were averaged for each mouse). Red line, piecewise exponential fit to the mouse-average density over 0.2–1 m, 1–3 m, and 3–4 m. Error bars: mean ± standard error across mice.

(E) Place field reliability over distance. Place cells were pooled across mice (and across trial types for day 4) then divided into 10 spatial bins based on their centers (shared limonene and pinene place cells were treated as two distinct place cells). The average value was computed for the place cells in each bin. Error bars: mean ± SEM Before and after odor training, place field reliability decreased with distance (two-sided Wilcoxon rank-sum test, day 0 $p = 1.3 \times 10^{-4}$, n = 146 0.1–2-m place cells versus n = 23 2–4-m place cells; day 4 $p = 1.9 \times 10^{-7}$, n = 748 0.1–2-m place cells versus n = 554 2–4-m place cells; STAR Methods). Following odor training, place field reliability increased (two-sided Wilcoxon rank-sum test, $p = 3.4 \times 10^{-6}$, n = 169 place cells for day 0 versus n = 1,302 place cells for day 4).

(F) Before and after odor training, the correlation between the trial-average vectors of population activity for even and odd trials of the same type decreased with distance (two-sided Wilcoxon rank-sum test, day 0 $p = 1.4 \times 10^{-12}$, n = 95 correlation values for 0.1–2 m versus n = 100 correlation values for 2–4 m; day 4 $p = 7.9 \times 10^{-16}$, n = 190 correlation values for 0.1–2 m versus n = 200 correlation values for 2–4 m; STAR Methods). Following odor training, population vector correlations increased (two-sided Wilcoxon rank-sum test, $p = 6.1 \times 10^{-36}$, n = 195 correlation values for day 0 versus n = 390 correlation values for day 4). Error bars: mean ± standard error across mice (and across trial types for day 4). *$p < 0.05$, **$p < 10^{-2}$, ***$p < 10^{-3}$.

(G) Single-trial activity of two neurons on day 4 from mouse m1. Left, limonene trials. Right, pinene trials.

(H) Trial-average activity of place cells across all mice, sorted by place field centers. Day 4, combined limonene and pinene trials (limonene- or pinene-specific place cell activities were averaged over trials of the appropriate type; shared limonene and pinene place cell activities were averaged over trials of both types).

(I) Cross-validation of place field ordering. Top, day 4, limonene trials. Bottom, day 4, pinene trials. Place cells were sorted by place field centers on odd trials. Left, odd-trial-average activity. Right, even-trial-average activity.

(J) Trial-average activity of neurons that meet place field criteria at both sites of odor presentation (1.2-2 m and 3.2-4 m) and excluded from place cell sorting on day 4, combined limonene and pinene trials.

(K) Correlation between fluctuations in the numbers of active places cells at the 1-m and 3-m odor cues. We plot the correlations in these z-scored quantities pooled across all trials for all mice (P values obtained via two-sided t test, P value = 7.9219e–13).

*$p < 0.05$, **$p < 10^{-2}$, ***$p < 10^{-3}$
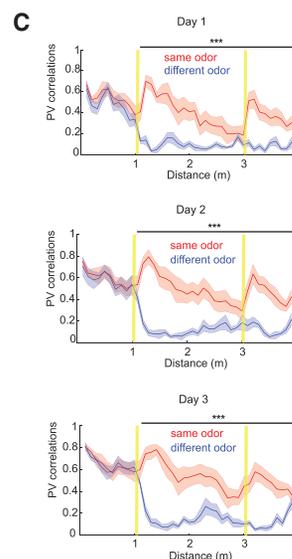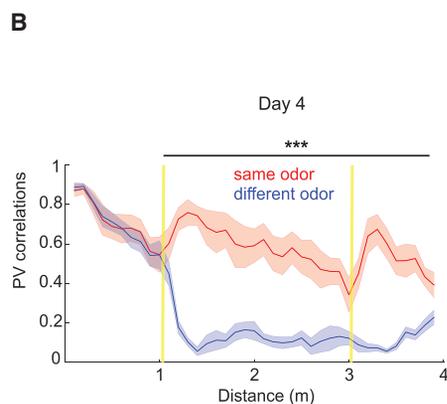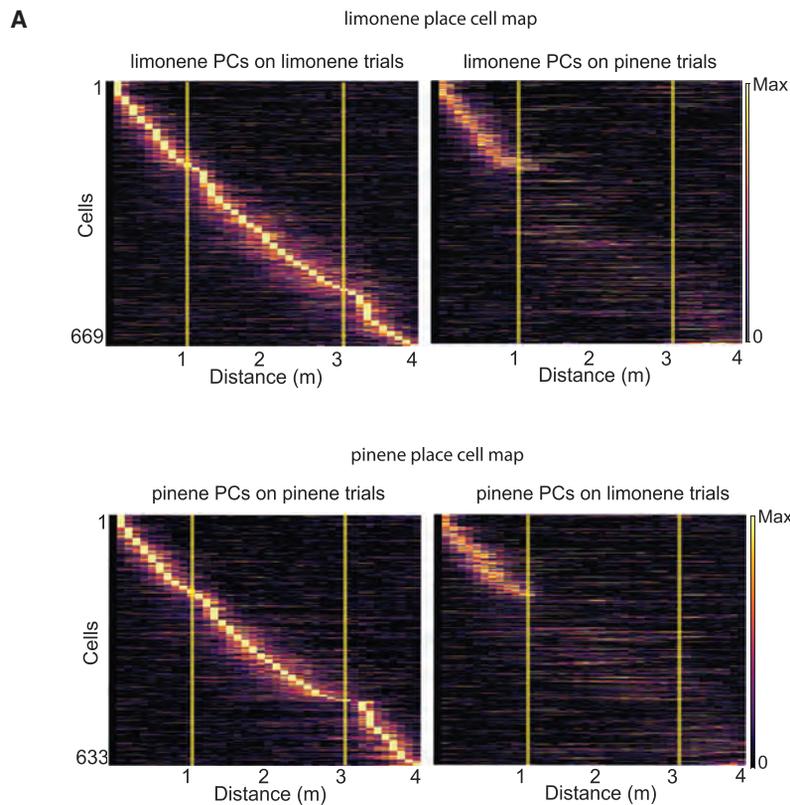
A

B

C

Figure 3. Olfactory landmarks induce place cell remapping and generate distinct cognitive spatial maps

(A) Remapping of the place cell representation on day 4. Top, trial-average activity of limonene place cells sorted by centers on limonene trials. Left, activity on limonene trials. Right, activity on pinene trials. Bottom, trial-average activity of pinene place cells sorted by centers on pinene trials. Left, activity on pinene trials. Right, activity on limonene trials.

(B) Red, correlation between trial-average vectors of population activity for even and odd trials of the same type on day 4 (same as in Figure 1F; STAR Methods). Blue, correlation between trial-average vectors of population activity for trials of different types on day 4 (STAR Methods). The different-odor population vector correlations were substantially reduced compared to the same-odor correlations beyond the 1-m odor cue (two-sided Wilcoxon rank sum test, p = 3.6 × 10^{-83}, n = 280 correlation values for each group). Error bars: mean ± standard error across mice.

(C) Population-level remapping. Same as (B), but for the first three days of odor training (days 1–3) rather than day 4. Top, day 1. Middle, day 2. Bottom, day 3. The different-odor population vector correlations were significantly smaller than the same-odor correlations beyond the 1-m odor cue for days 1–3 (two-sided Wilcoxon rank sum test, day 1 p = 1.2 × 10^{-65}, day 2 p = 1.3 × 10^{-70}, day 3 p = 9.9 × 10^{-75}, n = 280 correlation values for each group).

flected in the population-level activity in CA1. First, we analyzed population-level activity to study the gradual disambiguation of identical odor cues as distinct spatial landmarks. We computed the correlation between the trial-average vectors of population activity in 100-mm bins at locations x and $x + 2$ m (0.1 m $\leq x \leq 2$ m). Note that $x = 1$ m yields the correlation between the population vectors at the locations of the first and second odor cues. On the first day of training in the presence of odors, we observed a peak in population vector correlation immediately beyond $x = 1$ m, implying that the population vector at the second odor cue realigned to its state at the first odor cue (Figure 5A). Over the course of odor training, the correlation following $x = 1$ m was markedly diminished. Following odor training, the population response at the second odor

basic mechanism for extending cognitive spatial maps into unknown territory.

Population-level activity and state-space trajectories in CA1 reflect the gradual evolution of a cognitive spatial map

The gradual and sequential process by which the 1-m and 3-m odor cues were recognized as distinct landmarks was also re-

cue was uncorrelated with the response at the first odor cue (Figure 5A). This result is consistent with a spatial strategy rather than a strategy based upon sensory discrimination. In addition, we observe that over the course of 4 days of training with odor cues, the number of neurons that respond at both odor locations decreases more than 2-fold from day 1 to day 4 (Figures 5B, 5C, 5D, and 1J; 5.7%, 137 of 2405 neurons on day 1 to 2.4%, 68 of 2,778 neurons on day 4). Place fields
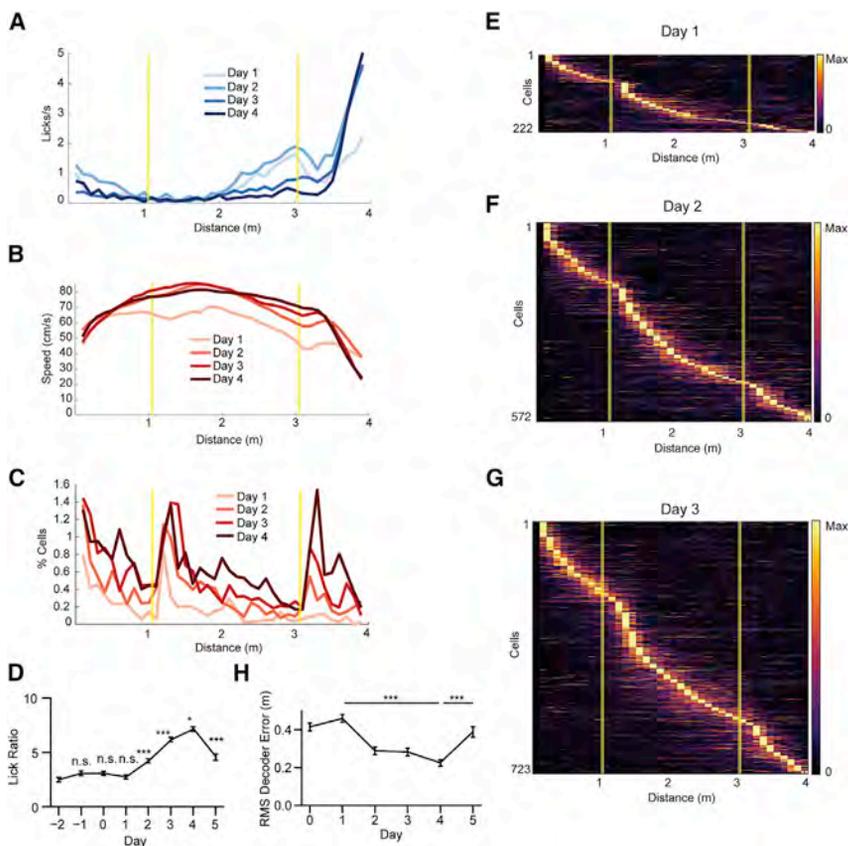
Figure 4. The gradual and sequential emergence of place cell maps and improvement in navigation behavior

(A and B) Trial- and mouse-average lick rate (A) and speed (B) over the course of odor training (days 1-4).

(C) Mouse-average spatial density of place cells over the course of odor training (days 1-4).

(D) Trial- and mouse-average lick ratio during pre-training (days −2 and −1) and Ca^{2+} imaging (days 0–5) (STAR Methods). On day 5, only trials with no odor cues are shown. During pre-training and the first day of odor training, the lick ratio did not change significantly across days (two-sided Wilcoxon rank-sum test, p = 5.8 × 10^{-2}, day −2 versus day −1; p = 1, day −1 versus day 0; p = 7.4 × 10^{-2}, day 0 versus day 1). By contrast, the lick ratio increased with each additional day of odor training (p = 1.4 × 10^{-9}, day 1 versus day 2; p = 3.7 × 10^{-10}, day 2 versus day 3; p = 1.4 × 10^{-2}, day 3 versus day 4). During day 5, on trials with no odor cues, the lick ratio decreased compared to day 4 (p = 6.6 × 10^{-11}; Bonferroni correction for 7 comparisons between adjacent days; n = 250 trials for days 1–4, n = 125 trials otherwise). Error bars: mean ± standard error across mice and trials.

(E–G) Trial-average activity of place cells across all mice, sorted by place field centers, for day 1 (E), day 2 (F), and day 3(G).

(H) Decoder error (root-mean-square) over the course of odor training. The error decreased through odor training (two-sided Wilcoxon rank-sum test, p = 4.4 × 10^{-25}, day 0 versus day 4) and increased once odors were removed on day 5 (two-sided Wilcoxon rank-sum test, p = 6.5 × 10^{-12}, day 4 versus day 5). Trial counts same as in c. Error bars: mean ± standard error across mice and trials.

*p < 0.05, **p < 10^{-2}, ***p < 10^{-3}

unique to the 1-m odor cue location are present at first day of training, whereas place fields unique to the 3-m odor emerge after several days of training. At this time, the population level activity is decorrelated and the number of neurons that respond at both odor cue locations has decreased substantially. Therefore, on the initial days of training the mice may have incorrectly recognized the distal odor cue at 3 m as the more proximal 1-m spatial landmark. Together, these data suggest that the two odor cues were gradually and sequentially recognized as spatial landmarks marking distinct locations.

We also performed principal component analysis (PCA) to study the state-space trajectory of neural population activity as the mice learned the task. Projecting the trial-average population state (combining neurons across mice) onto the first two PCA dimensions revealed a striking relationship between the structure of neural population activity and the structure of the task. Our virtual task has the topology of a circle because the mice 'return' to the start position on the next trial after reaching the reward location. After four days of odor training, the two-dimensional neural trajectory had the shape of a closed loop, and distances on the track were roughly proportional to corresponding distances along the neural trajectory (36.5% variance explained; Figures 5E, S5A, and S5B). Thus, the trajectory of this low-dimensional projection of population activity bears topological and metrical resemblance to the task.

We next examined the evolution of the neural trajectory during odor training. On the first day of odor exposure, the trajectory beyond the odor cue at 3 m loops back and retraces a path similar to the trajectory taken after the odor cue at 1 m (Figures 5F, S5B, and S5C). Also, the point on the trajectory corresponding to the reward location at 4 m was close to the point corresponding to 2 m. This trajectory is consistent with the misrecognition of the 3-m odor cue as the 1-m spatial landmark. Backward looping was reduced with training and by the fourth day was absent (Figures 5G and 5H). Thus, the decorrelation of the population responses evoked by the 1-m and 3-m odor cues is accompanied by a disentangling of the neural trajectory with relation to space.

Removal of odor cues or a rewarded location modifies place cell representations

We next asked whether the enriched place cell representation and improved navigational behavior that emerged during odor training persist in the absence of odor cues. On day 5, following 4 days of odor training, the mice performed a session in which pinene trials were randomly interleaved with no-odor trials (Figure 6A). We compared the place cell representations observed during no-odor trials on day 5 to no-odor trial on day 0. Although the number of place cells was larger (Figures 6B and 6C), and the licking behavior more accurate (Figures 6D) on day 5 than on day 0, the density of place cells decayed rapidly with a length constant only
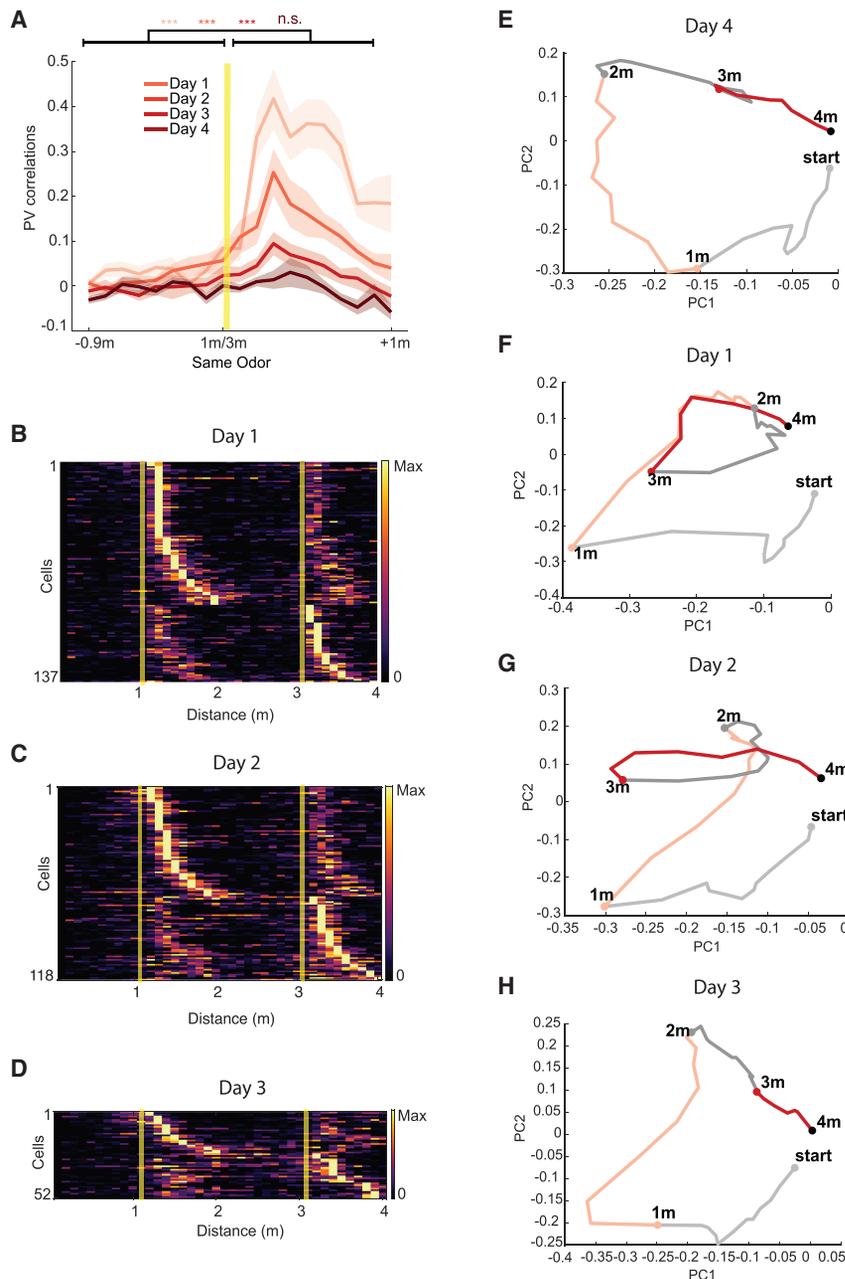
Figure 5. Population level activity and state-space trajectories in CA1 reflect the gradual evolution of a cognitive spatial map.

(A) Correlation between population vectors at corresponding 0.1–2 m and 2.1–4 m spatial bins as a function of distance from the 1-m or 3-m odor cues. On days 1–3, population vector correlations peak following the odor location (two-sided Wilcoxon rank-sum test, day 1 $p = 1.5 \times 10^{-21}$; day 2 $p = 3.9 \times 10^{-9}$; day 3 $p = 2.7 \times 10^{-4}$; n = 190 correlation values for −0.9–0 m versus n = 200 correlation values for 0–1 m). By day 4, the peak following the odor location was suppressed ($p = 0.39$). Error bars: mean ± standard error across mice and trial types.

(B–D) Trial-average activity of neurons that meet place field criteria at both sites of odor presentation (1.2-2 m and 3.2-4 m) and excluded from place cell sorting, combined limonene and pinene trials. (B) day 1 odor training. (C) day 2 odor training. (D) day 3 odor training.

(E–H) Trial-average state-space trajectories of neural population activity during the task, visualized in the leading 2 PCA dimensions (neurons combined across mice). (E) Day 4, pinene trials. (F) Day 1, pinene trials. (G) Day 2, pinene trials. (H) Day 3, pinene trials.

$^*p < 0.05$, $^{**}p < 10^{-2}$, $^{***}p < 10^{-3}$

ter reward was not delivered (Figure 6H). Under these conditions, the mice ran at similar speeds but did not lick or stop at 4 m (Figures 6I and 6J). The proportion of place cells decreased from 35% to 0.7% (29 of 3,919 neurons, 18 on limonene trials and 11 on pinene trials; Figure 6K; see Table S1D for significance tests). Thus, the robust place cell representation in our task is contingent on the presence of the reward. The absence of place cells when the reward is withheld may reflect the loss of spatial information provided by the reward cue or a lack of task motivation.

A model for the convergence of path integration and odor landmarks in place cell formation

The observation that odor cues can serve as navigational landmarks motivated a model to explain how the convergence of path integration and odor cues generates a cognitive spatial map in the hippocampus. The model consists of a population of place cells driven by inputs from a set of path integrators, and feedback from the place cells back to the path integrators (Figure 7A; STAR Methods). In the absence of odor cues, each path integrator generates an independent estimate of the distance that the animal has traveled from the starting point, and each estimate drives a different spatially modulated input to the place cells.

In our model, each path integrator samples a velocity estimate on each trial from a distribution centered at the animal's

slightly greater than observed on day-0 length constant ± bootstrapped standard error: 1.45 ± 0.18 m; one-sided bootstrap test versus day-0 length constant ± bootstrapped standard error: 0.97 ± 0.20 m, $p = 3.7 \times 10^{-2}$).

We also compared the place cell representation of day-5 trials with odor cues to the representation of trials without odor. The number of place cells beyond 2 m was 2.4 times greater on day-5 trials with odor cues than on trails without odor (308 versus 128 of 3,087 neurons, Figures 6E and 6F). In addition, the anticipatory licking was less accurate on day-5 trials without odor cues (Figure 6G).

We next explored the dependence of place cell activity on reward. On day 6, the mice performed a session in which the wa-
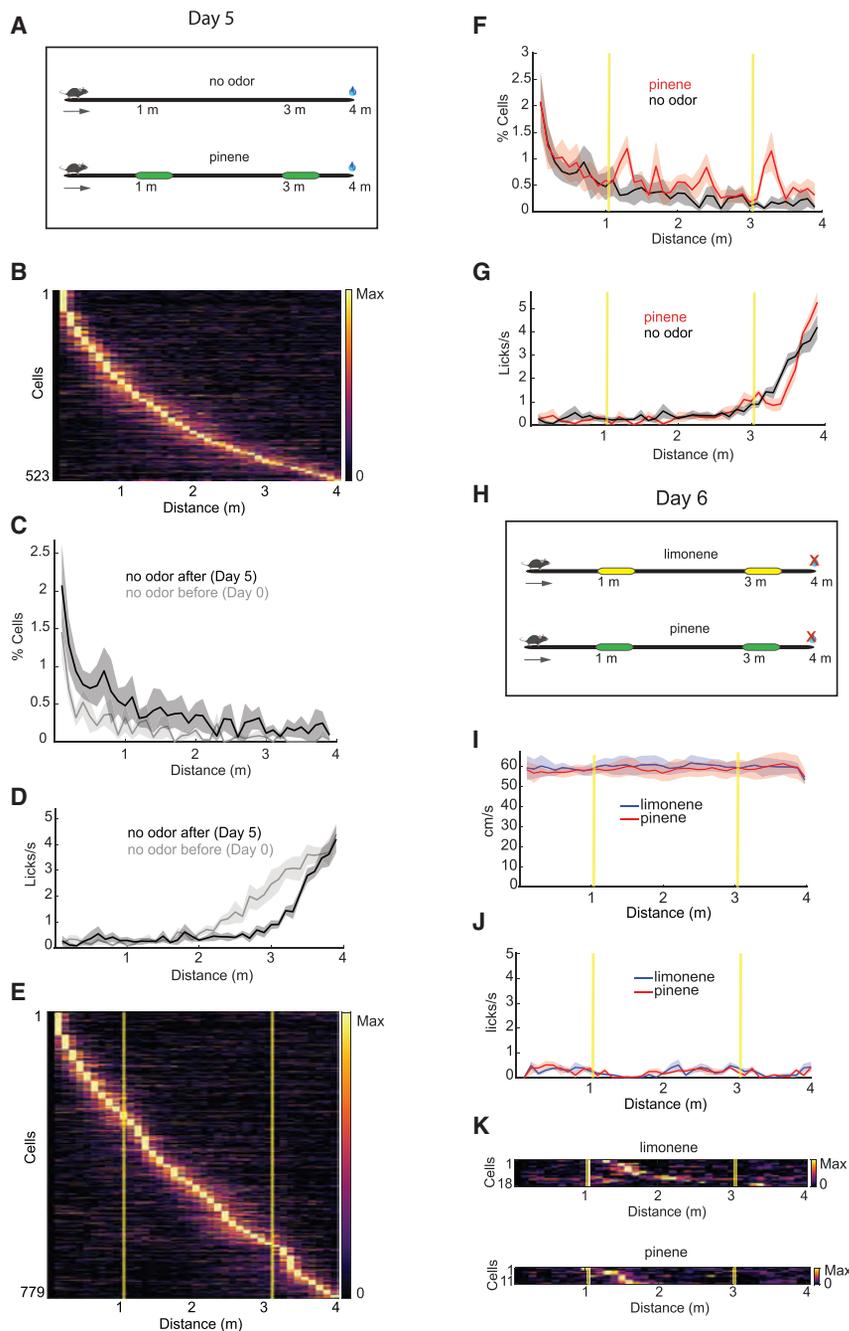
mation (Bittner et al., 2015; Bittner et al., 2017; Magee and Grienberger, 2020). The model posits that, in each cell, a plateau potential occurs at a random location, resulting in plasticity that sets the weights of the synapses from the integrators to that place cell to values proportional to the presynaptic input at the time of the plateau. Following this plasticity, the cell performs template matching, responding if there is a sufficiently close match between the current input rates and the rates experienced at the time of the plateau. This process creates reliable place cells at short distances from the starting location because the inputs driven by path integration are similar from trial to trial at these locations and therefore well matched to the template. For large distances, on the other hand, inputs vary considerably from trial to trial, rarely match the template, and reliable place cells cannot form. We chose a level of noise for the path integrators so that reliable place cells form only at distance less than 2 m (Figure 7C).

Model place cells project back to the path integrators, and this projection is also subject to plasticity. At the same time that plasticity modifies synapses from path integrators to a place cell, it

true velocity which, for simplicity, was modeled as being the same on each trial. To model variability in path integrator dynamics, we introduce noise into the velocity integral. Due to both velocity uncertainty and integration noise, the path integrators' estimates of position and, consequently, the inputs they drive vary from trial to trial. The trial-to-trial variance grows with the distance traveled as path integration becomes less reliable (Figures 7B).

Model place cells form by a process that simulates the effects of plateau potentials observed during CA1 place cell for-

A

Path Integrators   Place Cells

Odor Landmark

B

C

D
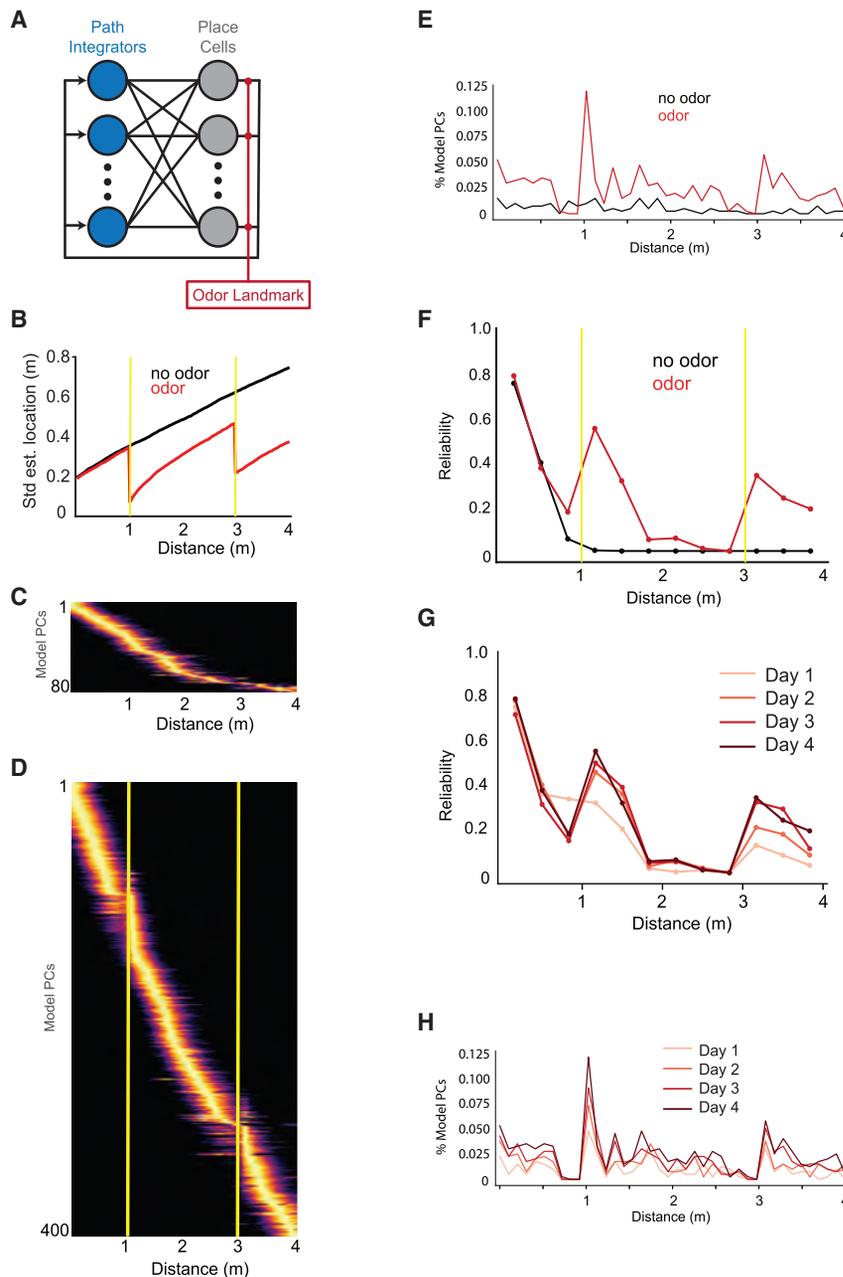

E

F

G

H

Figure 7. A model for the convergence of path integration and odor landmarks in place cell formation

(A) Schematic of the computational model. A population of noisy path integrators drives a population of place cells, which form reciprocal connections onto the path integrators. Odor cues gate the connections from place cells onto path integrators.

(B) The trial-to-trial variability of the position estimates of model path integrators grows monotonically with distance in the absence of odor cues (black) and is reduced at the locations of the odor cues due to resetting of the path integrators by the place cells (red).

(C) Without odor cues, few model place cells form beyond ∼2 m.

(D) In the presence of odor cues, model place cells tile the entire 4-m track.

(E) Spatial density of model place cells. Black, no odor cues on initial day of training (day 0). Red, after 4 training sessions in the presence of odor cues (day 4).

(F) Reliability of model place cells as a function of distance along the 4-m track. Black, no odor cues on initial day of training (day 0). Red, after 4 training sessions in the presence of odor cues (day 4).

(G) Reliability of model place cells as a function of distance along the 4-m track over the course of training. Lighter to darker shades or red indicate successive days of training in the presence of odor cues.

(H) Spatial density of model place cells over the course of training. Lighter to darker shades of red indicate successive days of training in the presence of odor cues.

also modifies connections from this place cell back to the path integrators. This plasticity stores a trace of the distance estimate provided by each path integrator at the time of the plateau. The result is a projection by which the activity of a place cell can reset a path integrator back to the value it took when the place field formed. In our model, this projection is only engaged when a sensory cue, the odor, appears (Figure 7A). Other work suggests that this one-shot plasticity rule could be replaced by a form of slow-timescale Hebbian plasticity (Ocko et al., 2018).

In the model, when an odor appears, place cell activity drives the path integrators to their previously stored values (Figure 7B). Although these values are no more accurate than the estimates

of distance on any other trial, they are consistent from trial to trial due to the reset provided by the odor-activated place cells. Thus, place cells that form beyond the 2-m point have inputs that are more reliable as a consequence of the odor cues. This consistency allows reliable place cells to be created beyond 2 m by the plateau potential mechanism. This process is then repeated at the location of the 3-m odor cue in an iterative process that enables a complete place cell representation along the entire 4-m track (Figure 7D).

The system we have described consists of two networks—the place cells and the path integrators—that store within their synapses the traces of their relationship at the time of place cell formation. Place cells are maximally driven by path integrators that match the input that occurred when their place fields formed. Reciprocally, place cell inputs to each path integrator store the value that the path integrator had when the place field formed. This system is calibrated by an external event that identifies when these relationships are consistent. This event is a landmark.

This model is also consistent with our experimental observations. First, in the model and in our experimental data following

odor training, equivalent sensory inputs presented at different locations activate distinct subpopulations of place cells. In the model, this occurs because only the place cells active when an odor cue is encountered are involved in resetting the path integrators and this, in turn, strongly drives a location-specific set of place cells in the vicinity of the cue. This is consistent with the role of the hippocampus in the transformation of egocentric sensory information into an allocentric cognitive spatial map of the external world. Second, the model predicts that place cell density and reliability (STAR Methods) decrease as a function of distance from odor cues, with local peaks in density and reliability at the site of each cue (Figures 7E and 7F). This is a consequence of model place cells being driven by a population of path integrators with independently accumulating errors. If path integration is implemented by grid cells in the MEC (McNaughton et al., 2006), as has been widely suggested, these independent path integrators could correspond to distinct grid modules (Stensola et al., 2012). In addition, the model predicts that the reliability of place cells along the entire track will improve with training in the presence of odor cues (Figures 7F and 7G). Both of these model predictions are in agreement with our experimental data (Figures 2D and 2E).

Finally, the iterative mechanism of spatial map extension posited by the model is consistent with our experimental findings regarding the evolution of place cell representations over the course of training. The model predicts that the same sensory cue presented at two different locations leads to the formation of local peaks in place cell density in an iterative and sequential manner (Figure 7H). In both the model and our data, a peak in place cell density initially emerges at the sensory cue nearest the start (1 m), and over several training sessions, the place cell map tiles the gap between 1 m and 3 m, eventually forming a second peak at 3 m (Figure 4C). Interestingly, our model predicts that an odor cue cannot be recognized as a landmark within an extant cognitive spatial map if its distance from a proximal cue is much greater than the decay length scale of the place cell representation, which is approximately 2 m.

DISCUSSION

For most organisms, olfaction is the central sensory modality by which they communicate with their environment. We have examined the role of olfaction in the generation of a cognitive spatial map essential for navigation. The interaction of path integration and visual landmarks in the control of place cells and navigation has been extensively studied (Poucet et al., 2014; Savelli and Knierim, 2019). However, interpretation is complicated by the fact that visual features (real or virtual) can be seen at a distance, have inherent spatial dimensions, and can be used to estimate velocity using optic flow and parallax motion. Previous studies have established that olfactory cues in concert with path integration, in the absence of visual information, can support place cell representations in the hippocampus (Radvansky and Dombeck, 2018; Save et al., 2000; Zhang and Manahan-Vaughan, 2015). In these studies, the odor cues were either not confined to a specific location or were presented as spatial gradients over a virtual track. Therefore, the specific contributions of sensory cues and path integration in the formation of the place cell representations were not clearly discernible. We have recorded the activity of a large number of neurons in CA1 during an olfactory-guided navigation task with localized odor cues and observed the process by which internal path integration imposes a spatial meaning onto an odor cue to create a landmark. This experimental paradigm allowed us to observe the convergence of olfactory information and internal path integration signals in the hippocampus during the emergence of place cell representations. The emergence of these place cell representations correlated with an increase in the accuracy of navigational behavior.

First, we found that internal path integration alone, in the absence of sensory cues, cannot support stable place fields or accurate navigation over distances longer than ~2 m from the start of the virtual track. As the animal moves further from the start landmark, the rapid decline in place cell density is consistent with the accumulation of errors in the internal path integration signals. The presentation of an odor cue at 1 m leads to the formation of a new peak in place fields at that location and thus a new spatial landmark. Different odors at the same 1-m distance along the track result in the activation of different place cell ensembles. Therefore, the spatial representations generated by olfactory landmarks do not represent distance alone but instead the convergence of path integration and olfactory sensory features.

In addition, we observe that the enhanced place cell representation generated by odor cues at 1 m leads to an increase in the density of place fields beyond 1 m. This implies that the number of place cells active at one location influences the number of place cells active at subsequent locations. In the absence of new sensory information, this influence diminishes as the path integrator becomes progressively less accurate. Place field densities show a qualitatively similar rapid decrease as a function of distance from either the start location or from the location of olfactory landmarks. Thus, the presence of olfactory cues appears to reset internal path integration signals.

The ability of an odor cue to serve as a spatial landmark depends on the accuracy of the path integrator at positions leading up to the odor location. When the same odor cue is present at two different locations, 1 m and 3 m, the cue nearest the starting position is the first to generate a unique place cell representation and appears to reset the path integrator. Over several days of training, place fields are generated that span the gap between the two spaced, but identical, odor cues. Only then does the odor cue at 3 m generate a distinct place cell representation and an additional peak in the density of place fields at 3 m. The gradual and sequential extension of place fields over the entire virtual track and the improvement in navigational accuracy reflect the disambiguation of two identical odor cues as distinct spatial landmarks. Thus, the same sensory features present at multiple locations can be identified as unique landmarks by an iterative process that relies on path integration.

Our experiments demonstrating that path integration and odor cues interact to form a cognitive spatial map in CA1 motivated a model in which reciprocally connected path integrators and place cells generate spatial selectivity via bidirectional plasticity. The model we propose explains how place cell ensembles in the hippocampus can be generated at the site of spatial landmarks through the coincidence of localized odor information and

reliable path integration signals. The high dimensionality that results from a place cell ensemble code implies that a very large number of unique landmarks can be represented in the hippocampus. In addition, our model posits that a landmark representation in the hippocampus improves the accuracy of path integration signals via direct feedback projections to the MEC.

Previous models describing the interaction of landmarks and path integration require dedicated landmark cells (Campbell et al., 2018; Ocko et al., 2018). Our model does not assume the pre-existence of cells dedicated to the recognition and representation of landmarks as abstract spatial features. Instead, the model postulates that landmark-related activity arises in the hippocampus through the convergence of sensory and path integration signals. This leads to the recognition and representation of a given sensory feature as a spatial landmark and then informs path integration circuits through feedback and plasticity mechanisms.

In conclusion, we have combined CA1 population recordings with theoretical modeling to provide evidence for a process in which odor cues serve as landmarks that reset noisy path integrators, enabling the iterative expansion of a cognitive spatial map in the hippocampus. The convergence of path integration and olfactory landmarks in the hippocampus allows mice to construct spatial maps that support navigation over distances far greater than would be possible with path integration alone.

STAR★METHODS

Detailed methods are provided in the online version of this paper and include the following:

- KEY RESOURCES TABLE
- RESOURCE AVAILABILITY
  - Lead contact
  - Materials availability
  - Data and code availability
- EXPERIMENTAL MODEL AND SUBJECT DETAILS
- METHOD DETAILS
  - Surgeries
  - Virtual odor-guided navigation system
  - Measurement of time-varying odorant dynamics
  - Behavior training
  - Reward delivery
  - Imaging and behavioral data collection
  - Processing of imaging data
  - Behavioral data processing and alignment to neural activity
  - Spatial binning and selection of trials for analysis
  - Behavioral quantification (lick ratio and lick rate center of mass)
  - Place cell analysis
  - Characterization of place cell quality (reliability, jitter, and width)
  - Correlation between fluctuations in the numbers of active places cells at the 1-m and 3-m odor cues
  - Population vector analyses
  - Position decoding
  - Reversion to the mean velocity analysis
  - A model of place cells driven by and interacting with path integrators
  - Statistical analysis

AUTHOR CONTRIBUTIONS

W.M.F., R.A., L.F.A, and M.J.S. designed the experiments. W.M.F. and N.R.J. performed the experiments. W.M.F., D.G.C., and V.D. performed the analysis. D.G.C. and L.F.A. performed computational modeling. L.J.K. and M.J.S. designed a calcium signal extraction algorithm used for the initial analysis of the imaging data. W.M.F., D.G.C., R.A., L.F.A., and M.J.S. wrote the paper, and all authors commented on the manuscript.

DECLARATION OF INTERESTS

M.J.S. is a scientific co-founder of Inscopix, which produces the miniature fluorescence microscope used in this study.

REFERENCES

Aboitiz, F., and Montiel, J.F. (2015). Olfaction, navigation, and the origin of isocortex. Front. Neurosci. 9, 402. https://doi.org/10.3389/fnins.2015.00402.

Aikath, D., Weible, A.P., Rowland, D.C., and Kentros, C.G. (2014). Role of self-generated odor cues in contextual representation. Hippocampus 24, 1039–1051. https://doi.org/10.1002/hipo.22289.

Anderson, M.I., and Jeffery, K.J. (2003). Heterogeneous modulation of place cell firing by changes in context. J. Neurosci. 23, 8827–8835.

Baker, K.L., Dickinson, M., Findley, T.M., Gire, D.H., Louis, M., Suver, M.P., Verhagen, J.V., Nagel, K.I., and Smear, M.C. (2018). Algorithms for Olfactory Search across Species. J. Neurosci. 38, 9383–9389. https://doi.org/10.1523/JNEUROSCI.1668-18.2018.

Barretto, R.P., Ko, T.H., Jung, J.C., Wang, T.J., Capps, G., Waters, A.C., Ziv, Y., Attardo, A., Recht, L., and Schnitzer, M.J. (2011). Time-lapse imaging of disease progression in deep brain areas using fluorescence microendoscopy. Nat. Med. 17, 223–228. https://doi.org/10.1038/nm.2292.

Bittner, K.C., Grienberger, C., Vaidya, S.P., Milstein, A.D., Macklin, J.J., Suh, J., Tonegawa, S., and Magee, J.C. (2015). Conjunctive input processing drives feature selectivity in hippocampal CA1 neurons. Nat. Neurosci. 18, 1133–1142. https://doi.org/10.1038/nn.4062.

Bittner, K.C., Milstein, A.D., Grienberger, C., Romani, S., and Magee, J.C. (2017). Behavioral time scale synaptic plasticity underlies CA1 place fields. Science 357, 1033–1036. https://doi.org/10.1126/science.aan3846.

Bourboulou, R., Marti, G., Michon, F.X., El Feghaly, E., Nouguier, M., Robbe, D., Koenig, J., and Epsztein, J. (2019). Dynamic control of hippocampal spatial coding resolution by local visual cues. eLife 8, e44487. https://doi.org/10.7554/eLife.44487.

Campbell, M.G., Ocko, S.A., Mallory, C.S., Low, I.I.C., Ganguli, S., and Giocomo, L.M. (2018). Principles governing the integration of landmark and self-motion cues in entorhinal cortical codes for navigation. Nat. Neurosci. 21, 1096–1106. https://doi.org/10.1038/s41593-018-0189-y.

Chen, G., King, J.A., Burgess, N., and O'Keefe, J. (2013). How vision and movement combine in the hippocampal place code. Proc. Natl. Acad. Sci. USA 110, 378–383. https://doi.org/10.1073/pnas.1215834110.

Diodato, A., Ruinart de Brimont, M., Yim, Y.S., Derian, N., Perrin, S., Pouch, J., Klatzmann, D., Garel, S., Choi, G.B., and Fleischmann, A. (2016). Molecular signatures of neural connectivity in the olfactory cortex. Nat. Commun. 7, 12238. https://doi.org/10.1038/ncomms12238.

Draht, F., Zhang, S., Rayan, A., Schönfeld, F., Wiskott, L., and Manahan-Vaughan, D. (2017). Experience-dependency of reliance on local visual and idiothetic cues for spatial representations created in the absence of distal information. Front. Behav. Neurosci. 11, 92. https://doi.org/10.3389/fnbeh.2017.00092.

Etienne, A.S., and Jeffery, K.J. (2004). Path integration in mammals. Hippocampus 14, 180–192. https://doi.org/10.1002/hipo.10173.

Etienne, A.S., Maurer, R., Berlie, J., Reverdin, B., Rowe, T., Georgakopoulos, J., and Séguinot, V. (1998). Navigation through vector addition. Nature 396, 161–164. https://doi.org/10.1038/24151.

Etienne, A.S., Maurer, R., Boulens, V., Levy, A., and Rowe, T. (2004). Resetting the path integrator: A basic condition for route-based navigation. J. Exp. Biol. 207, 1491–1508. https://doi.org/10.1242/jeb.00906.

Fattahi, M., Sharif, F., Geiller, T., and Royer, S. (2018). Differential representation of landmark and self-motion information along the CA1 radial axis: self-motion generated place fields shift toward landmarks during septal inactivation. J. Neurosci. 38, 6766–6778. https://doi.org/10.1523/JNEUROSCI.3211-17.2018.

Friedrich, J., Zhou, P., and Paninski, L. (2017). Fast online deconvolution of calcium imaging data. PLoS Comput. Biol. 13, e1005423. https://doi.org/10.1371/journal.pcbi.1005423.

Ghosh, K.K., Burns, L.D., Cocker, E.D., Nimmerjahn, A., Ziv, Y., Gamal, A.E., and Schnitzer, M.J. (2011). Miniaturized integration of a fluorescence microscope. Nat. Methods 8, 871–878. https://doi.org/10.1038/nmeth.1694.

Grieves, R.M., Jenkins, B.W., Harland, B.C., Wood, E.R., and Dudchenko, P.A. (2016). Place field repetition and spatial learning in a multicompartment environment. Hippocampus 26, 118–134. https://doi.org/10.1002/hipo.22496.

Hafting, T., Fyhn, M., Molden, S., Moser, M.B., and Moser, E.I. (2005). Microstructure of a spatial map in the entorhinal cortex. Nature 436, 801–806. https://doi.org/10.1038/nature03721.

Hamburger, K., and Knauff, M. (2019). Odors can serve as landmarks in human wayfinding. Cogn. Sci. (Hauppauge) 43, e12798. https://doi.org/10.1111/cogs.12798.

Hardcastle, K., Ganguli, S., and Giocomo, L.M. (2015). Environmental boundaries as an error correction mechanism for grid cells. Neuron 86, 827–839. https://doi.org/10.1016/j.neuron.2015.03.039.

Igarashi, K.M., Lu, L., Colgin, L.L., Moser, M.B., and Moser, E.I. (2014). Coordination of entorhinal-hippocampal ensemble activity during associative learning. Nature 510, 143–147. https://doi.org/10.1038/nature13162.

Jacobs, L.F. (2012). From chemotaxis to the cognitive map: the function of olfaction. Proc. Natl. Acad. Sci. USA 109 (Suppl 1), 10693–10700. https://doi.org/10.1073/pnas.1201880109.

Jacobs, L.F., Arter, J., Cook, A., and Sulloway, F.J. (2015). Olfactory orientation and navigation in humans. PLoS ONE 10, e0129387. https://doi.org/10.1371/journal.pone.0129387.

Jayakumar, R.P., Madhav, M.S., Savelli, F., Blair, H.T., Cowan, N.J., and Knierim, J.J. (2019). Recalibration of path integration in hippocampal place cells. Nature 566, 533–537. https://doi.org/10.1038/s41586-019-0939-3.

Jeffery, K.J. (1998). Learning of landmark stability and instability by hippocampal place cells. Neuropharmacology 37, 677–687.

Kim, I.S., and Dickinson, M.H. (2017). Idiothetic Path Integration in the Fruit Fly Drosophila melanogaster. Curr.Biol. 27, 2227–2238.E3. https://doi.org/10.1016/j.cub.2017.06.026.

Koutsoklenis, A., and Papadopoulos, K. (2011). Olfactory Cues Used for Wayfinding in Urban Environments by Individuals with Visual Impairments. J. Vis. Impair. Blind. 105, 692–702. https://doi.org/10.1177/0145482X1110501015.

Kropff, E., Carmichael, J.E., Moser, M.B., and Moser, E.I. (2015). Speed cells in the medial entorhinal cortex. Nature 523, 419–424. https://doi.org/10.1038/nature14622.

Kulvicius, T., Tamosiunaite, M., Ainge, J., Dudchenko, P., and Wörgötter, F. (2008). Odor supported place cell model and goal navigation in rodents. J. Comput. Neurosci. 25, 481–500. https://doi.org/10.1007/s10827-008-0090-x.

Leitner, F.C., Melzer, S., Lütcke, H., Pinna, R., Seeburg, P.H., Helmchen, F., and Monyer, H. (2016). Spatially segregated feedforward and feedback neurons support differential odor processing in the lateral entorhinal cortex. Nat. Neurosci. 19, 935–944. https://doi.org/10.1038/nn.4303.

Li, Y., Xu, J., Liu, Y., Zhu, J., Liu, N., Zeng, W., Huang, N., Rasch, M.J., Jiang, H., Gu, X., et al. (2017). A distinct entorhinal cortex to hippocampal CA1 direct circuit for olfactory associative learning. Nat. Neurosci. 20, 559–570. https://doi.org/10.1038/nn.4517.

MacDonald, C.J., Carrow, S., Place, R., and Eichenbaum, H. (2013). Distinct hippocampal time cell sequences represent odor memories in immobilized rats. J. Neurosci. 33, 14607–14616. https://doi.org/10.1523/JNEUROSCI.1537-13.2013.

Magee, J.C., and Grienberger, C. (2020). Synaptic Plasticity Forms and Functions. Annu. Rev. Neurosci. 43, 95–117. https://doi.org/10.1146/annurev-neuro-090919-022842.

Marin, A.C., Schaefer, A.T., and Ackels, T. (2021). Spatial information from the odour environment in mammalian olfaction. Cell Tissue Res. 383, 473–483. https://doi.org/10.1007/s00441-020-03395-3.

McNaughton, B.L., Battaglia, F.P., Jensen, O., Moser, E.I., and Moser, M.B. (2006). Path integration and the neural basis of the 'cognitive map'. Nat. Rev. Neurosci. 7, 663–678. https://doi.org/10.1038/nrn1932.

Mittelstaedt, M.-L., and Mittelstaedt, H. (1980). Homing by Path Integration in a Mammal. Naturwissenschaften 67, 566–567. https://doi.org/10.1007/Bf00450672.

Mittelstaedt, M.L., and Mittelstaedt, H. (2001). Idiothetic navigation in humans: estimation of path length. Exp. Brain Res. 139, 318–332. https://doi.org/10.1007/s002210100735.

Müller, M., and Wehner, R. (1988). Path integration in desert ants, Cataglyphis fortis. Proc. Natl. Acad. Sci. USA 85, 5287–5290. https://doi.org/10.1073/pnas.85.14.5287.

Müller, M., and Wehner, R. (2010). Path integration provides a scaffold for landmark learning in desert ants. Curr. Biol. 20, 1368–1371. https://doi.org/10.1016/j.cub.2010.06.035.

Muzzio, I.A., Levita, L., Kulkarni, J., Monaco, J., Kentros, C., Stead, M., Abbott, L.F., and Kandel, E.R. (2009). Attention enhances the retrieval and stability of visuospatial and olfactory representations in the dorsal hippocampus. PLoS Biol. 7, e1000140. https://doi.org/10.1371/journal.pbio.1000140.

Nosal, A.P., Chao, Y., Farrara, J.D., Chai, F., and Hastings, P.A. (2016). Olfaction Contributes to Pelagic Navigation in a Coastal Shark. PLoS ONE 11, e0143758. https://doi.org/10.1371/journal.pone.0143758.

Ocko, S.A., Hardcastle, K., Giocomo, L.M., and Ganguli, S. (2018). Emergent elasticity in the neural code for space. Proc. Natl. Acad. Sci. USA 115, E11798–E11806. https://doi.org/10.1073/pnas.1805959115.

Porter, J., Craven, B., Khan, R.M., Chang, S.J., Kang, I., Judkewitz, B., Volpe, J., Settles, G., and Sobel, N. (2007). Mechanisms of scent-tracking in humans. Nat. Neurosci. 10, 27–29. https://doi.org/10.1038/nn1819.

Poucet, B., Sargolini, F., Song, E.Y., Hangya, B., Fox, S., and Muller, R.U. (2014). Independence of landmark and self-motion-guided navigation: a different role for grid cells. Philos. Trans. R. Soc. Lond. B Biol. Sci. *369*, 20130370. https://doi.org/10.1098/rstb.2013.0370.

Quirk, G.J., Muller, R.U., and Kubie, J.L. (1990). The firing of hippocampal place cells in the dark depends on the rat's recent experience. J. Neurosci. *10*, 2008–2017.

Radvansky, B.A., and Dombeck, D.A. (2018). An olfactory virtual reality system for mice. Nat. Commun. *9*, 839. https://doi.org/10.1038/s41467-018-03262-4.

Radvansky, B.A., Oh, J.Y., Climer, J.R., and Dombeck, D.A. (2021). Behavior determines the hippocampal spatial mapping of a multisensory environment. Cell Rep. *36*, 109444. https://doi.org/10.1016/j.celrep.2021.109444.

Raithel, C.U., and Gottfried, J.A. (2021). Using your nose to find your way: Ethological comparisons between human and non-human species. Neurosci. Biobehav. Rev. *128*, 766–779. https://doi.org/10.1016/j.neubiorev.2021.06.040.

Ravassard, P., Kees, A., Willers, B., Ho, D., Aharoni, D.A., Cushman, J., Aghajan, Z.M., and Mehta, M.R. (2013). Multisensory control of hippocampal spatiotemporal selectivity. Science *340*, 1342–1346. https://doi.org/10.1126/science.1232655.

Sargolini, F., Fyhn, M., Hafting, T., McNaughton, B.L., Witter, M.P., Moser, M.B., and Moser, E.I. (2006). Conjunctive representation of position, direction, and velocity in entorhinal cortex. Science *312*, 758–762. https://doi.org/10.1126/science.1125572.

Save, E., Cressant, A., Thinus-Blanc, C., and Poucet, B. (1998). Spatial firing of hippocampal place cells in blind rats. J. Neurosci. *18*, 1818–1826.

Save, E., Nerad, L., and Poucet, B. (2000). Contribution of multiple sensory information to place field stability in hippocampal place cells. Hippocampus *10*, 64–76. https://doi.org/10.1002/(SICI)1098-1063(2000)10:1<64:AID-HIPO7>3.0.CO;2-Y.

Savelli, F., and Knierim, J.J. (2019). Origin and role of path integration in the cognitive representations of the hippocampus: computational insights into open questions. J. Exp. Biol. *222* (Pt, Suppl 1), jeb188912. https://doi.org/10.1242/jeb.188912.

Sosulski, D.L., Bloom, M.L., Cutforth, T., Axel, R., and Datta, S.R. (2011). Distinct representations of olfactory information in different cortical centres. Nature *472*, 213–216. https://doi.org/10.1038/nature09868.

Steck, K., Hansson, B.S., and Knaden, M. (2009). Smells like home: Desert ants, Cataglyphis fortis, use olfactory landmarks to pinpoint the nest. Front. Zool. *6*, 5. https://doi.org/10.1186/1742-9994-6-5.

Stensola, H., Stensola, T., Solstad, T., Frøland, K., Moser, M.B., and Moser, E.I. (2012). The entorhinal grid map is discretized. Nature *492*, 72–78. https://doi.org/10.1038/nature11649.

Stettler, D.D., and Axel, R. (2009). Representations of odor in the piriform cortex. Neuron *63*, 854–864. https://doi.org/10.1016/j.neuron.2009.09.005.

Taxidis, J., Pnevmatikakis, E.A., Dorian, C.C., Mylavarapu, A.L., Arora, J.S., Samadian, K.D., Hoffberg, E.A., and Golshani, P. (2020). Differential Emergence and Stability of Sensory and Temporal Representations in Context-Specific Hippocampal Sequences. Neuron *108*, 984–998.e9. https://doi.org/10.1016/j.neuron.2020.08.028.

Woods, N.I., Stefanini, F., Apodaca-Montano, D.L., Tan, I.M.C., Biane, J.S., and Kheirbek, M.A. (2020). The Dentate Gyrus Classifies Cortical Representations of Learned Stimuli. Neuron *107*, 173–184.e6. https://doi.org/10.1016/j.neuron.2020.04.002.

Wu, Y., Chen, K., Ye, Y., Zhang, T., and Zhou, W. (2020). Humans navigate with stereo olfaction. Proc. Natl. Acad. Sci. USA *117*, 16065–16071. https://doi.org/10.1073/pnas.2004642117.

Young, B.J., Otto, T., Fox, G.D., and Eichenbaum, H. (1997). Memory representation within the parahippocampal region. J. Neurosci. *17*, 5183–5195.

Zhang, S., and Manahan-Vaughan, D. (2015). Spatial olfactory learning contributes to place field formation in the hippocampus. Cereb. Cortex *25*, 423–432. https://doi.org/10.1093/cercor/bht239.

Zhang, S., Schönfeld, F., Wiskott, L., and Manahan-Vaughan, D. (2014). Spatial representations of place cells in darkness are supported by path integration and border information. Front. Behav. Neurosci. *8*, 222. https://doi.org/10.3389/fnbeh.2014.00222.eCollection.

Zhao, X., Wang, Y., Spruston, N., and Magee, J.C. (2020). Membrane potential dynamics underlying context-dependent sensory responses in the hippocampus. Nat. Neurosci. *23*, 881–891. https://doi.org/10.1038/s41593-020-0646-2.

Zhou, P., Resendez, S.L., Rodriguez-Romaguera, J., Jimenez, J.C., Neufeld, S.Q., Giovannucci, A., Friedrich, J., Pnevmatikakis, E.A., Stuber, G.D., Hen, R., et al. (2018). Efficient and accurate extraction of in vivo calcium signals from microendoscopic video data. eLife *7*, e28728. https://doi.org/10.7554/eLife.28728.

Ziv, Y., Burns, L.D., Cocker, E.D., Hamel, E.O., Ghosh, K.K., Kitch, L.J., El Gamal, A., and Schnitzer, M.J. (2013). Long-term dynamics of CA1 hippocampal place codes. Nat. Neurosci. *16*, 264–266. https://doi.org/10.1038/nn.3329.

STAR★METHODS

KEY RESOURCES TABLE

REAGENT or RESOURCE	SOURCE	IDENTIFIER
Experimental models: Organisms/strains		
Mouse: wild type C57BL/6J	Jackson Laboratory	000664; RRID:IMSR_JAX:000664
Software and algorithms		
nVista Acquisition Software	Inscopix, inc.	Version 2.0
Mosaic	Inscopix, in.	1.1.1b; RRID:SCR_017408
CNMF-E	Zhou et al., 2018	https://github.com/zhoupc/CNMF_E
OASIS	Friedrich et al., 2017	https://github.com/j-friedrich/OASIS
MATLAB	Mathworks	https://www.mathworks.com/products/matlab.html; RRID:SCR_001622
Arduinio IDE	Arduino	https://www.arduino.cc/en/software
Python 3.6	Python	https://www.python.org/; RRID:SCR_008394
iPython and Jupyter		https://jupyter.org/; RRID:SCR_018414
Custom analysis code	Python	https://doi.org/10.5281/zenodo.5526602
Other		
pENN.AAV.CamKII.GCaMP6f.WPRE.SV40	Addene	100834-AAV1
GRIN lens 1.00mm diameter, 4.0mm length	Inscopix, inc.	Part ID:1050-004595
Miniature fluorescent microscope	Inscopix, inc.	nVista v2.0; RRID:SCR_017407

RESOURCE AVAILABILITY

Lead contact
Further information and requests for resources should be directed to and will be fulfilled by the lead contact, Dr. Richard Axel (ra27@columbia.edu).

Materials availability
This study did not generate new unique reagents.

Data and code availability
Original data have been deposited to Mendeley Data:
"Fischler-Ruiz2021," Mendeley Data, V1, https://doi.org/10.17632/62zmrvt6jy.1
The code used for analysis is available at:
https://doi.org/10.5281/zenodo.5526602

EXPERIMENTAL MODEL AND SUBJECT DETAILS

We report data here from 5 adult male (8-12 weeks old) C57BL/6J mice acquired from Jackson Laboratory. Mice were individually housed and maintained on a 12 hour reverse light/dark cycle. All experiments were conducted during the dark cycle when mice are most active. All experiments and surgical protocols were performed in accordance with the guide of Care and Use of Laboratory Animals (NIH) and were approved by the institutional Animal Care and Use Committee at Columbia University.

METHOD DETAILS

Surgeries
Mice underwent two surgical procedures under isoflurane (1%–2% vol/vol). We injected ~500 nL of a 1:3 dilution in PBS of AAV2/1 serotype virus expressing GCaMP6f under the control of the CaMKII promoter (UPENN Vector Core, AAV1.CamKII.GCaMP6f. WPRE.SV40, titer $1–3 \times 10^{13}$ vg/ml) with a thin glass pipette into the left hemisphere of dorsal CA1 (–2.2 mm from bregma, 1.6 mm mediolateral, –1.2 mm dorsoventral). 1–2 weeks after viral injection we implanted a 1.8 mm diameter imaging cannula

(metal cannula with a glass coverslip attached at the bottom, Inscopix part number 1050-002189) over the dorsal surface of CA1 centered on the site of viral injection after aspiration of the overlying cortical area as previously described(Barretto et al., 2011). We then secured the cannula and a custom metal head bar to the cranium of the mice using dental cement (Dentsply). 1–2 weeks after cannula implantation we inserted a 1 mm diameter gradient refractory index (GRIN) micro-endoscope (Inscopix part number 1050-002176) into the cannula and a plastic baseplate (Inscopix part number 1050-002192) was cemented into place after confirming even expression of GCaMP6f in healthy tissue using a miniaturized fluorescent microscope (Inscopix nVista, v2.0).

Virtual odor-guided navigation system

Mice were head-fixed on a spherical treadmill (20-cm diameter Styrofoam ball) rotating on a single axis. The axis of the treadmill was attached to an analog rotary encoder (US Digital part number MA3-A10-125-B) connected to an Arduino Mega2560. Angular displacement was converted to a linear distance based on the circumference of the treadmill. A water port consisting of a small gavage needle (Cadence Science part number 7901) connected to a water reservoir was placed within reach of the mouse's tongue. A capacitance touch sensor (Sparkfun part number MPR121) was attached to the water port to measure licking and the sensor was connected to the Arduino Mega2560. Small 2–4 μL drops of water were delivered by the brief opening a solenoid valve (Lee Valves part number LHDA 12712154) connected to the water port. Custom Arduino software was used to deliver water drops at reward locations. Limonene and pinene odor cues were delivered via a custom olfactometer controlled by an Arduino Mega2560. 10% solutions of limonene (Sigma part number 183164) and pinene (Sigma part number P45680) diluted in mineral oil (Fisher Scientific part number 0121-1) were added to syringe filters (Whatman part number 6888-2527) and an additional filter of pure mineral oil was used to provide blank odor stimuli between the 1 s presentations of limonene and pinene cues. Custom Arduino software was used to control odor valves for switching between limonene or pinene and blank (mineral oil) filters. Two mass flow controllers (MFCs) were used to maintain a constant airflow of compressed medical grade air for odor delivery. One MFC was set to deliver air to the odor and blank filters at 0.3 L/min. The other MFC was set at 0.7 L/min to deliver clean air for a carrier stream. The combined airflow experienced by the mouse was a constant 1 L/min in the absence or presence of limonene and pinene odor cues. The odor or blank air streams and the carrier stream were combined in an 8-port odor manifold (Island Motion Corporation 020206.0001) connected to one side of a custom odor port that was placed within 2 mm of the nose. A vacuum was connected to the opposite side of the odor port. The vacuum line was controlled by an MFC set at 1 L/min to remove air and odor continuously from the odor port. Speakers delivering white noise at 70 dB were placed in front of the mouse to cancel out ambient noise and the sound of the valves opening and closing. The entire experimental system was enclosed by black hard-board (Thorlabs part number TB4) on the sides, Blackout nylon fabric (Thorlabs part number BK5) on the top, and the lights were kept off in the room to maintain a dark environment. Mice were monitored using an IR camera (Basler A601f) and illuminated using an IR light.

Measurement of time-varying odorant dynamics

Odor concentrations were measured using a photoionization detector (miniPID 201A Aurora Scientific) placed in the airstream that was used to deliver odors to the nose of the mice. The 0–10 V output of the PID was converted to a normalized concentration range plotted in arbitrary units. Measurements were done with the exact same dilutions of odor used in all of the experiments: 10% dilutions of either limonene or pinene in mineral oil. Flow rates were matched to those used in all experiments: 0.3 L/min odor source combined with a constant 0.7 L/min or clean air.

Behavior training

After surgeries, the mice were placed on a 12-hour reverse light/dark cycle. All experiments were performed in the middle of the active (dark) period. The mice were habituated to handling for several days. The mice were then habituated to head-fixation on the spherical treadmill for several days before being put on water restriction. After 2–3 days on water restriction (∼2 mL water per day), the mice were trained to walk increasing linear distances to receive water rewards. On the initial day of training, the distance to reward was set at 0.5 m. After the mice were able to complete > 60 trials in one 20-min session (1 session per day) the distance was gradually increased from 0.5 to 1 m, then from 1 m to 4 m in 1 m increments. After graduating to the 4-m track, the mice were required to complete ≥ 80 trials in a single 20-min session for 3 consecutive days, at which point we began collecting the data for these experiments. The 5 mice used in this study achieved these criteria after 4–11 days of training at 4 m.

Reward delivery

Rewards consisted of 2–4 μL drops of water. The delivery of the first reward is triggered when the mice reach 4 m. No licking is required for the first reward. Each additional reward is triggered by two licks. This design allows the mice to control reward delivery and avoids a buildup of water at the port. After reaching 4 m, the mice are free to progress on the treadmill and trigger rewards for a period of 4 s. After 4 s, rewards cease and the next trial begins. Additionally, if the mice traverse more than 1 m within the 4 s period, rewards cease and the next trial begins (rare). The number of rewards was variable as mice triggered water drops themselves, excluding the first drop. On each trial, 5–15 drops were typically delivered. Note that there is no explicit signal for the start of each trial other than cessation of the water reward.

Imaging and behavioral data collection

At the beginning of each experimental session, mice were head fixed on the spherical treadmill and the miniature microscope (Inscopix, v2.0) was attached to the plastic baseplate. The field of view containing GCamp6f-expressing neurons was examined to confirm that the site was aligned with previous recording sessions. Imaging data were collected at a frame rate of 20 Hz. LED power was set between 30%–40%. The data were initially collected at a resolution of 1440 × 1080 pixels and then subsequently down-sampled by a factor of 4 for further analysis.

Processing of imaging data

Calcium imaging movies were preprocessed using the Mosaic software package (Inscopix). During preprocessing, movies were spatially cropped to fit the imaging site and motion corrected. Individual neurons were isolated using the publicly available CNMF-E MATLAB package(Zhou et al., 2018). The calcium signals extracted using CNMF-E were then deconvolved using the publicly available OASIS algorithm(Friedrich et al., 2017). The inferred activity yielded by OASIS (denoted by s in OASIS) was used for analysis in this study.

Behavioral data processing and alignment to neural activity

We used custom Arduino software to convert rotary encoder signals to a virtual linear distance and speed was calculated over rolling 200 ms time windows. Lick detection from touch sensor signals was aligned to virtual distances. A TTL pulse was sent to the Arduino Mega2560 from the microscope on the acquisition of each imaging frame to align neural activity to virtual distance, speed, and licking. Signals for the opening and closing of odor and water reward valves were recorded by Arduino Mega2650 and aligned to behavior and activity data.

Spatial binning and selection of trials for analysis

For all analyses except for decoding-related analyses, aligned behavioral and imaging data were averaged within spatial bins of 100 mm on each trial, yielding a total of 40 spatial bins. We excluded the first bin (0–100 mm) to limit our analyses to periods when the mice were actively running toward the reward location. In all analyses, we excluded any data after initiation of the initial water reward, so all licking shown is pre-reward. Because there was no explicit signal for the start of the experiment other than the termination of the water reward, several 4 m reward crossings were typically required before mice showed engagement with the task. Thus, the first 5 trials for each trial type in a session were excluded. We analyzed trials 6–30 for each trial type. During pre-training, the mice performed sessions with > 60 trials, but only trials 6–30 were analyzed for consistency with Ca^{2+} imaging sessions.

Behavioral quantification (lick ratio and lick rate center of mass)

To quantify behavioral performance, we computed a lick ratio using the spatially binned lick rate. On each trial, we computed the ratio of the mean lick rate over the last 3 spatial bins (3.7–4 m) to the mean lick rate over the last 30 spatial bins (1–4 m). Thus, the lick ratio is unity when licking is uniform across the track and maximized (lick ratio = 10) when licking is withheld until 3.7–4 m. The first 10 spatial bins (0–1 m) were excluded from the analysis since, toward the beginning of the track, mice often continued to lick following the most recent reward. To assess the dependence of licking behavior on trial-to-trial velocity deviations, we computed the center of mass of the spatially binned lick rate on each trial, excluding the first 10 spatial bins (0–1 m) from the computation.

Place cell analysis

Place cells were classified using the spatially binned neural data according to the following procedure. First, the track was divided into 4 approximately equal-length segments: 0.1–1.1 m, 1.1–2 m, 2–3.1 m, and 3.1–4 m. These segments consisted of 10, 9, 11, and 9 spatial bins, respectively (for a total of 39 bins rather than 40, since the first bin was excluded from analysis). Candidate place cells had at least one segment in which two criteria were simultaneously satisfied: (1) a bin had trial-average activity greater than 3 times the trail-average activity over the whole track, and (2) a bin had z-scored activity greater than 1 in more than 25% of trials (7 or more trials). We z-scored neural activity prior to spatial binning. If condition (1) was met in both the 1.1–2 m and 3.1–4 m segments and the bin of peak trial-average activity fell in one of these ranges, the cell was not classified as a place cell (such neurons are described in the text as 'neurons that responded at both sites of odor presentation'). Otherwise, the cell was classified as a place cell. This procedure selects cells with consistent spatially localized activity. A place field's center was taken to be the spatial bin with peak trial-average activity, excluding the first bin.

To assess the false-positive rate of our place cell selection procedure, we performed shuffling tests. To shuffle the data, we used both circular permutations, which preserved the spatial autocorrelation of each neuron's activity, as well as arbitrary permutations, which destroyed all spatial structure. These methods resulted in similar shuffled distributions of place cell counts (Figure S1F). On shuffled data, our procedure selected 1–2 orders of magnitude fewer place cells than on unshuffled data. No shuffles yielded more place cells than yielded by unshuffled data. We conclude that the false-positive rate of our procedure is low, and that the place cell counts reported in the text are significant with respect to shuffled distributions.

We also performed a test specifically designed to reveal a potential bias against selecting place cells at boundaries between 1-m bins (Figure S1G). Using circular spatial shifts, we moved the bin of peak trial-average activity for each cell to either 1 m or 3 m.

As a result, all place cells selected by our procedure had centers at 1 m or 3 m. Rather than drastically reducing the number of place cells, shifting the data yielded slightly larger numbers of place cells. It is therefore unlikely that the proposed bias affected our results.

Characterization of place cell quality (reliability, jitter, and width)

Place field reliability was defined as the fraction of trials on which the z-scored activity for a given place cell was greater than unity within ± 1 spatial bin (100 mm) of the place cell's center. Neural activity was z-scored prior to spatial binning. For artificial place cells in our computational model, place field reliability was defined as the fraction of trials on which a place cell had activity greater than a threshold (0.15) at its central location. Place field jitter was defined as the root-mean-square difference between a place field's center and its center on single trials (location of peak single-trial activity). For jitter computation, activity outside of ± 10 spatial bins of a place field's center was zeroed out, and trials on which a cell was not active within ± 10 bins of the center were excluded from the calculation. Finally, to avoid confusing jitter with place field expansion, we computed width on a single-trial basis. On each trial, we computed a width by dividing the sum-total activity by the peak activity. These single-trial values were then averaged across trials to obtain a place field's width. As in the computation of jitter, activity outside of ± 10 spatial bins of a place field's center was zeroed out, and trials on which a cell was not active within ± 10 bins of the center were excluded from the calculation.

Correlation between fluctuations in the numbers of active places cells at the 1-m and 3-m odor cues

On a given trial, we defined the number of place cells active at the 1-m (3-m) odor cue to be the number of place cells with centers between 1.2 m and 2 m (3.2 and 4 m) whose z-scored activity was greater than one within +- 1 bins of the center bin (0.1 m bins). We z-scored this quantity within each mouse, odor type, and location (i.e., 1 m or 3 m). We plot the correlations in these z-scored quantities for each mouse and pooled across mice.

Population vector analyses

The stability of the vector of population activity across trials was computed as follows. First, using the spatially binned neural data, we computed the even- and odd-trial-average population vectors at each spatial bin. Then, we computed at each bin the element-wise Pearson correlation between the two vectors. To analyze remapping, we performed a similar analysis, but computed the element-wise correlation between the even-trial-average population vectors for different odor types. To analyze the gradual orthogonalization of the population responses evoked by the 1-m and 3-m odor cues, we computed the correlation between the trial-average population vectors at locations x and $x + 2$ m for 0.1 m $\leq x \leq 2$ m, as described in the main text. The first bin (0–100 mm) was excluded from this analysis as usual.

Position decoding

We used a naive Bayesian decoder to decode position from neural activity. In the signal extracted from the Calcium imaging data, each neuron's activity is related to its true spiking activity by an unknown proportionality constant. However, the value of zero is non-arbitrary and corresponds to the neuron being silent. We therefore performed the decoder analysis on binarized neural data, assigning '1' to time bins where the inferred activity was positive and '0' otherwise. Time bins were 50 ms, corresponding to the 20 Hz imaging frame rate. We modeled the i-th neuron's activity, denoted by n_i, using a Bernoulli spiking model with a position-dependent spike probability denoted by $r_i(x)$. That is, $p(n_i|x) \sim \text{Bernoulli}(r_i(x))$. In turn, $r_i(x)$ was given as the spike probability (across training set trials) of the i-th neuron at position x, where position was binned in 50 mm bins, and the trial-average activity was smoothed using a Gaussian kernel ($\sigma = 0.2$ m). In bins in which $r_i(x)$ was less than a minimum spike probably p_{min}, we set $r_i(x) = p_{min}$, a form of regularization ($p_{min} = 10^{-4}$). We used 15 bins of neural activity (total of 750 ms), centered at the current time step, to decode position at each time step. The key assumption of the naive Bayesian decoder is that neural responses are conditionally independent given position, so that $p(n_{1:N}|x) = \prod_i p(n_i|x)$. The decoded position estimate at time t was computed as $\hat{x}_t = \text{arg max}_x \, p(x|n_{1:N}) = \text{arg max}_x \, p(n_{1:N}|x)$, assuming a uniform prior on position. We used leave-one-out cross validation. On days with two odor conditions (days 1–4), we fit the decoder using only trials of the same odor condition. Thus, the decoder was always fit using 24 trials and evaluated on one. We began decoding at 100 mm.

Reversion to the mean velocity analysis

We computed the error of the decoder on the i-th trial as $\varepsilon_i = \frac{1}{T_i} \int_0^{T_i} \left(x_{dec,i}(t) - x_i(t) \right) dt$, where $x_{dec,i}(t)$ is the decoder output, $x_i(t)$ is the mouse's actual position, and T_i is the duration of the i-th trial. Thus, ε_i is positive when the decoder overestimates position on average and negative when the decoder underestimates position on average. Note that we use the RMS decoder error, rather than the 'signed' error described here, to measure the overall performance of the decoder. The velocity deviation on the i-th trial was computed as $\Delta v_i = v_i - v_{avg}$, where $v_i = (3.9$ m$)/T_i$ and $v_{avg} = (\Sigma_i v_i)/25$. We used 3.9 m instead of 4 m since this analysis excluded the first 100 mm of the track. To obtain the slope of the relationship between decoder errors and velocity deviations corresponding to a total reliance on the average velocity, we computed each ε_i by using the trial-average position for the decoder output: $x_{dec,i}(t) = (\Sigma_i x_i(t))/25$. Then, we fit a line to the relationship between the resulting ε_i's and Δv_i's and extracted the fitted slope.

A model of place cells driven by and interacting with path integrators

Model place cells receive inputs that are modulated by a set of locations estimated by path integration (Figure 7a). All of the model place cells receive the same set of 100 spatially tuned inputs with firing rates $f_i(x_i)$ for $i = 1, 2, ..., 100$. Each function f_i is generated initially by a Gaussian random process, using a Gaussian kernel with length constant 0.35 m, and then held fixed. Each variable $x_i(t)$ is an independent noisy estimate of the location of the animal at time t, obtained by integrating a noisy estimate of the animal's velocity with added white-noise fluctuations. Specifically, on each trial, velocities for these integrators are chosen from a Gaussian distribution around the true velocity of the animal, taken to be 0. 4 m/s, with a standard deviation of 0.05 m/s. In addition, Gaussian white noise was added to the integrated velocity, configured to produce a standard deviation of 0.175 m after 1 s. This causes each x_i to differ from the others on every trial and also to vary from trial to trial. As a result, the modulated inputs, $f_i(x_i(t))$, are also different and vary from trial to trial. These fluctuations increase as a function of t as the animal moves along the virtual track because the integrator-to-integrator and trial-to-trial variance of the location estimates increases as a function of the integration interval. Additionally, each integrator is randomly initialized at the starting location using a zero-mean Gaussian with standard deviation 0.2 m.

The input to place cell a, for $a = 1, 2, ..., 150$, is $\Sigma_i w_{ai} f_i(x_i(t))/|f(x(t))|$, where the expression in the denominator is the norm of the vector with components $f_i(x_i(t))$, and w_{ai} is the weight of the input from integrator i to place cell a. A threshold of 0.55 is subtracted from this input, and the place cells firing rate, $r_a(t)$, is determined by rectifying the result. Independent Gaussian noise with standard deviation 0.055 is applied to each place cell's threshold at each time step.

When a place cell is subject to plasticity, we choose a time t_a^* for this plasticity to take place, simulating the effects of a dendritic plateau potential(Bittner et al., 2015; Bittner et al., 2017). We denote the values of the path integrators at this time and on this trial by $x_i^*(t_a^*)$. The result of this plateau is that the weights to model place cell a are set to $w_{ai} = f_i(x_i^*(t_a^*))/|f(x^*(t_a^*))|$, i.e., the input at time of the plateau. Following this plasticity, the input to place cell a is equal to the cosine of the angle between the vector $f(x^*(t_a^*))$ (the input vector at time t^* on the trial when the plasticity occurred) and the vector $f(x)$ at the current time on the current trial. If the place cell happened to form near the start of the virtual track, it is likely that it will fire on subsequent trials because the vector $f(x)$ only fluctuates by a small amount from trial to trial when the integrators only have to integrate over a short distance. If, on the other hand, the place cell formed at a larger distance from the start, the larger fluctuations in $f(x)$ from trial to trial cause a poor match to the weights and, as a result, the place cell is unlikely to fire. This is the reason that reliable place cells only form across the first 2 m of the virtual track.

For comparison with our experimental data, we ran the model using artificial notions of days and trials. We used 5 artificial days with 80 artificial trials per day. Odor landmarks were present on all days except the first. On each trial, 3 cells have plateau potentials. If such a cell is active on the next trial, its status as a place cell is cemented and it is no longer subject to plasticity. Otherwise, it becomes subject to plasticity once again. On each day, a maximum of 80 place cells can form. Using the parameter settings described here, all 80 place cells successfully formed on each day.

Thus far, we have described the connections from the path integrators to the place cells, but there are connections from place cells to path integrators in the model as well (Figure 7a), and these are also plastic. When plasticity acts on the inputs to place cell a, we imagine that it also acts on the inputs from that place cell back to the path integrators. This is assumed to be similar to the plasticity discussed in reference(Campbell et al., 2018), but we do not model this circuit in full, focusing instead on the results of this plasticity. The effect of this plasticity is that the value $x^*_i(t_a^*)$ is stored in synapses from place cell a to a path integrator i. Specifically, if an odor is present at time t_{odor}, which we assume gates the effect of place cells on the path integrators (Figure 7a), path integrator i is reset to $x_i(t_{odor}) = \Sigma_a x^*_i(t_a^*) r_a(t_{odor})/\Sigma_a r_a(t_{odor})$. The result of this resetting is that, after the odor appears, the trial-to-trial variability of the path integrator estimates is greatly reduced. This consistency produces a better match between the weight vectors of place cells formed beyond the odor location and the input vectors generated by the path integrators. The result is that reliable place cells can now form along the entire virtual track (Figure 6E).

Statistical analysis

Data analysis and computational modeling were performed using MATLAB and Python.

To assess changes in place cell proportions, we used Pearson's x^2 tests. In cases where this test yielded a P value of exactly zero in MATLAB (using the 'chi2cdf' function), we report $p < 10^{-16}$. To assess the significance of correlations in Figures 2K and S1M we used two-sided t tests. To assess differences in a quantity between two unpaired groups, we used two-sided Wilcoxon rank-sum tests. To assess whether two fitted slopes were different, or whether a fitted slope was less or greater than some value, we used one-sided bootstrap tests with 10,000 bootstraps. In cases where no bootstraps were in favor of the null hypothesis, we report $p < 10^{-4}$. To fit an exponential function to place cell densities, we used a standard curve fitting function. We used 10,000 bootstraps to place error bars on length constants and to compare different length constants. In order to correct for multiple comparisons, we apply Bonferroni corrections by multiplying raw P values by the number of comparisons. In cases where this yielded a corrected P value greater than unity, we report $p = 1$. No statistical methods were used to predetermine sample sizes.